Biogeosciences, 21, 1433–1459, 2024
https://doi.org/10.5194/bg-21-1433-2024
© Author(s) 2024. This work is distributed under
the Creative Commons Attribution 4.0 License.

Biogeosciences Open Access EGU



# Oceanographic processes driving low-oxygen conditions inside Patagonian fjords

**Pamela Linford[1,2,3], Iván Pérez-Santos[2,3,4], Paulina Montero[3,4], Patricio A. Díaz[2,5], Claudia Aracena[6,7], Elías Pinilla[8,14], Facundo Barrera[9,10], Manuel Castillo[11], Aida Alvera-Azcárate[12], Mónica Alvarado[13], Gabriel Soto[8], Cécile Pujol[12], Camila Schwerter[2], Sara Arenas-Uribe[2], Pilar Navarro[2], Guido Mancilla-Gutiérrez[2], Robinson Altamirano[2], Javiera San Martín[8], and Camila Soto-Riquelme[8]**

[1]Programa de Doctorado en Ciencias, Mención Conservación y Manejo de Recursos Naturales, Universidad de Los Lagos, Puerto Montt, Chile
[2]Centro i-mar, Universidad de Los Lagos, Casilla 557, Puerto Montt, Chile
[3]Center for Oceanographic Research COPAS Sur-Austral and COPAS COASTAL, Universidad de Concepción, Concepción, Chile
[4]Centro de Investigación en Ecosistemas de la Patagonia (CIEP), Coyhaique, Chile
[5]CeBiB, Universidad de Los Lagos, Casilla 557, Puerto Montt, Chile
[6]Centro de Investigación en Recursos Naturales y Sustentabilidad, Universidad Bernardo O'Higgins, Avenida Viel 1497, Santiago, Chile
[7]Laboratorio Costero de Recursos Acuáticos de Calfuco, Universidad Austral de Chile, Valdivia, Chile
[8]Instituto de Fomento Pesquero (IFOP), CTPA Putemún, Castro, Chile
[9]Fundación Bariloche and CONICET, San Carlos de Bariloche, Argentina
[10]Centro Austral de Investigaciones Científicas (CADIC), CONICET, Bernardo Houssay 200, Ushuaia, Argentina
[11]Centro de Observación Marino para Estudios de Riesgos del Ambiente Costero, Universidad de Valparaíso, Valparaíso, Chile
[12]AGO-GHER, University of Liège, Liège, Belgium
[13]Servicio Hidrográfico y Oceanográfico de la Armada de Chile, Valparaíso, Chile
[14]Department of Civil and Environmental Engineering, University of Maine, Orono, ME, USA

**Correspondence:** Iván Pérez-Santos (ivan.perez@ulagos.cl)

Received: 10 April 2023 – Discussion started: 26 April 2023
Revised: 23 November 2023 – Accepted: 9 January 2024 – Published: 20 March 2024

**Abstract.** The dissolved oxygen (DO) levels of coastal ocean waters have decreased over the last few decades in part because of the increase in surface and subsurface water temperature caused by climate change, the reduction in ocean ventilation, and the increase in stratification and eutrophication. In addition, biological and human activity in coastal zones, bays, and estuaries has contributed to the acceleration of current oxygen loss. The Patagonian fjord and channel system is one world region where low-DO water (LDOW, 30 %–60 % oxygen saturation) and hypoxia conditions ( $< 30$ % oxygen saturation, 2 mL $L^{-1}$ or 89.2 µmol $L^{-1}$) are observed. An in situ dataset of hydrographic and biogeochemical variables (1507 stations), collected from sporadic oceanographic cruises between 1970 and 2021, was used to evaluate the mechanisms involved in the presence of LDOW and hypoxic conditions in northern Patagonian fjords. Results denoted areas with LDOW and hypoxia coinciding with the accumulation of inorganic nutrients and the presence of salty and oxygen-poor Equatorial Subsurface Water mass. The role of biological activity in oxygen reduction was evident in the dominance of community respiration over gross primary production. This study elucidates the physical and biogeochemical processes contributing to hypoxia and LDOW in the northern Patagonian fjords, highlighting the significance of performing multidisciplinary research and combining observational and modeling work. This approach underscores the

**Published by Copernicus Publications on behalf of the European Geosciences Union.**

importance of a holistic understanding of the subject, encompassing both real-world observations and insights provided by modeling techniques.

## 1 Introduction

Hypoxic conditions and low-dissolved-oxygen water (LDOW) have expanded globally over the last decade along coastal waters and oceans (Schmidtko et al., 2017; Breitburg et al., 2018). The origins of the hypoxia and LDOW are attributed to natural and anthropogenic processes. Remineralization of organic matter, weak circulation, extended residence time, and stratification were reported as natural processes (Rabalais et al., 2010; Bianchi et al., 2010). In contrast, water eutrophication was documented as one of the main anthropogenic processes. (Díaz et al., 2001; Conley et al., 2009; Meire et al., 2013). Therefore, for decades, the scientific community has been paying close attention to this issue because of the expected impacts on the survival, abundance, development, growth, reproduction, and behavior of the most important taxonomic groups at different stages of their life cycles, such as mollusks, crustaceans, and fish (Sampaio et al., 2021; Ekau et al., 2010; Batiuk et al., 2009; Vaquer-Sunyer and Duarte, 2008; Breitburg et al., 1997; Díaz and Rosenberg, 1995; Andrewartha and Birch, 1986; Davis, 1975), which could also affect all services provided to humans (Laffoley and Baxter, 2019).

Some examples of the impact of LDOW on biological behaviors are changes in the composition of benthic communities in prolonged periods of dissolved oxygen (DO) $< 4.2\,\mathrm{mL\,L^{-1}}$ (Ekau et al., 2010); negative impacts on the growth and abundance of cod ($3.6\,\mathrm{mL\,L^{-1}}$; 70 %); the limit of the distribution of sardine larvae ($2.6\,\mathrm{mL\,L^{-1}}$; 50 %); the distribution of jellyfish ($1.6\,\mathrm{mL\,L^{-1}}$; 30 %); and the decrease in the abundance, swimming capacity, and filtration of copepods ($0.52\,\mathrm{mL\,L^{-1}}$; 10 %), described by Ekau et al. (2010). Additionally, oxygen deficiency affects the growth rate and feed conversion efficiency and, in some species, even increases the concentration of toxic substances (Davis, 1975). In a Patagonian fjord used for recreational fishing of rainbow trout (*Salmo gairdneri*), values under 50 % saturation caused a reduction in swimming speed (Jones, 1971b) and altered respiration and metabolism (Kutty, 1968). In the case of coho salmon (*Oncorhynchus kisutch*), a commonly farmed species, a growth rate proportional to the oxygen level was observed for saturations between 40 % and 80 %, and the hypoxia modulated the transcriptional immunological response (Martínez et al., 2020). Finally, Pérez–Santos et al. (2018) reported habitat reduction of microzooplankton in a Patagonian fjord (Puyuhuapi Fjord) due to the presence of hypoxic conditions at depths below 100 m.

Throughout the world's oceans, there are areas in which the dissolved oxygen (DO) is significantly lower than in well-oxygenated areas (such as $< 20\,\mu\mathrm{M}$, $\sim 0.4$ or $0.31\,\mathrm{mL\,L^{-1}}$) as shown by Breitburg et al. (2018). These areas are known as oxygen minimum zones (OMZs). OMZs result from organic matter degradation, weak water circulation, long residence times, and weak ventilation (Fuenzalida et al., 2009). The major ocean OMZs are located in the eastern South Pacific, the Arabian Sea, the Bay of Bengal (Indian Ocean), the western Bering Sea, and the Gulf of Alaska, covering approximately 8 % of the total ocean or approximately $30 \times 10^6\,\mathrm{km^2}$ (Paulmier and Ruiz-Pino, 2009; Fuenzalida et al., 2009).

Along the Peru–Chile coastline, the eastern South Pacific (ESP) oxygen minimum zone (OMZ) extends poleward. As one moves southward, it gradually diminishes in both size and strength until it approaches the Patagonian fjord system (Silva et al., 2009). Recently, Linford et al. (2023) demonstrated poleward transport of hypoxic and LDOW of the Equatorial Subsurface Water (ESSW) mass alongside the Patagonian region. As the ESSW (originating in the equatorial region) moves south, it passes throughout the OMZ, carrying oxygen-poor water (89–134 µM) with high nitrate concentration (20–30 µM) and elevated salinity (34.9) (Silva et al., 2009). Studies of water masses inside Patagonian fjords and channels have detected the presence of the ESSW only in the northern region, between 41 and 45° S. This water mass enters the northern Patagonia region via the Guafo mouth (Fig. 1b), a deep channel with a depth of 150–200 m and width of 35 km (Sievers and Silva, 2008; Pérez-Santos et al., 2014; Schneider et al., 2014). The ESSW is one of the main causes of hypoxia and LDOW inside Patagonian fjords (e.g., Puyuhuapi Fjord and Jacaf Channel). Nevertheless, these conditions are also found in other areas where sills block the pass of the ESSW, e.g., the Reloncaví system (Reloncaví Fjord and Reloncaví Sound) and Aysén, Comau, and Quitralco fjords (Fig. 1) (Silva and Vargas, 2014; Linford et al., 2023; Díaz et al., 2023).

Regarding other processes favoring hypoxia and LDOW inside Patagonian fjords, Silva (2008) proposed biological processes that include the consumption of DO, such as respiration and the remineralization of organic matter. A high load of organic matter (autochthonous and allochthonous) in the water column and sediments increases DO consumption during microbial community respiration, contributing to the LDOW content in most of the Patagonian fjord headwaters (Castillo et al., 2016) as well as higher community respiration rates than primary production (Montero et al., 2011, 2017b). The main contributor to the increase in allochthonous organic matter is the river supplies, mainly during late winter and early spring, owing to the dominance of ice melt over precipitation during the winter season. The highest river discharges in the region are found in Puelo, Petrohué, and Cochamó rivers in the Reloncaví Fjord; the Cisnes River in the Puyuhuapi Fjord; and other freshwater contributions from small rivers in the northern Patagonian fjords (Castillo et al., 2016; Schneider et al., 2014). Additionally, weak deep ventilation and long residence times in fjord

waters are assumed to promote a reduction in the DO concentration (Schneider et al., 2014; Silva and Vargas, 2014).

The Patagonian fjord ecosystem is under substantial continued economic pressure due to salmon aquaculture and other economic activities (Billi et al., 2022). The northern Patagonian fjords (Fig. 1b, c) account for half of the national production and a significant number of salmon concessions (Billi et al., 2022). A risk analysis carried out in this region established that the Reloncaví estuarine system and the Comau, Puyuhuapi, Quitralco, and Cupquelán fjords are regions with an especially elevated level of risk for the development of harmful algal blooms (HABs) and eutrophication events, owing to the nutrient input by the intense aquaculture of salmon (Soto et al., 2021). Nevertheless, environmental studies on salmon farming have shown that this economic activity has a geographically limited impact because most nutrients are quickly recycled by biological processes in the water column (Soto and Norambuena, 2004).

Another meaningful impact of salmon production is the increase in allochthonous organic matter load, which, when combined with the high production of autochthonous organic matter by phytoplankton, favors a decrease in DO in the water column and sediments (Quiñones et al., 2019). Salmon farming supplies allochthonous dissolved substrates through the dissolution of organic particles derived from feces and uneaten feed (Wang et al., 2012). This organic material is considered highly degradable (Nimptsch et al., 2015; Montero et al., 2022), promoting enhanced rates of heterotrophic bacterial activity (e.g., bacterial production (BP) and extracellular enzymatic activity (EEA); Montero et al., 2022).

The main goal of this study was to analyze the processes contributing to hypoxia and LDOW in northern Patagonia, such as ESSW advection, DO consumption during the use of organic matter (community respiration), biogeochemical processes, deep-water ventilation, and residence times of water inside fjords. A combination of the in situ dataset, primary-production experiments, and modeling results were used to demonstrate the occurrence of processes promoting low-oxygen conditions in the northern Patagonian fjords.

## 2 Materials and methods

### 2.1 Hydrographic and chemical data

A total of 1507 stations were used to describe northern Patagonia's hydrographical and chemical processes; 593 stations were sampled during the fall–winter seasons and 914 during the spring–summer seasons (Table 1). Most temperature and salinity records were obtained using a CTD (conductivity, temperature, and depth profiler) instrument (e.g., SBE 19plus, SBE 15, and AML Metrec•XL). When SBE CTDs were used, data were processed according to the manufacturer's protocol and software (SBE Data Processing). When using the AML CTD, the raw data underwent quality control, eliminating records out of range according to historical CTD data (Pérez-Santos et al., 2014, 2021; Linford et al., 2023), after which the data were averaged every 1 m. Additionally, membrane and optical sensors (e.g., SBE 43 and Optode 4831) together with the Winkler method have been used to obtain DO data (Strickland and Parsons, 1968). Experiments were conducted to validate the CTD DO data with the Winkler method, showing satisfactory results and high statistical correlation ($R^2$ range of 0.92–0.99, figure not included).

Figure 1b and c show the station positions during fall–winter and spring–summer. The absolute salinity ($S_A$ in $g\,kg^{-1}$) and conservative temperature ($\Theta$ in °C) were calculated using the Thermodynamic Equation of SeaWater 2010 (TEOS-10) (IOC et al., 2010). In TEOS-10, absolute salinity represents the spatial variation in the composition of seawater, considering the different thermodynamic properties and gradients of horizontal density in the open ocean. Conservative temperature is similar to potential temperature but represents the heat content of seawater with greater precision.

A temperature–salinity ($T$–$S$) diagram was constructed based on the conservative temperature and absolute salinity values and was used to identify and quantify the water masses in the Patagonian fjords using only the salinity criteria proposed by Sievers (2008) and Sievers and Silva (2008). In Patagonian fjords, the density features of the water column are dominated by the vertical–horizontal distribution of the salinity rather than the water temperature, justifying the use of salinity in the identification of water masses (Aiken, 2012; Pérez-Santos et al., 2014). According to this classification, Estuarine Water (EW, 0–31 $g\,kg^{-1}$) originates in the surface layer owing to the water supply from rivers and summer time glacier melting. Below the EW, a Modified Subantarctic Water (MSAAW, salinity 31–33 $g\,kg^{-1}$) layer is located from the mixing of the EW with the Subantarctic Water (SAAW, salinity 33–33.8 $g\,kg^{-1}$). Finally, an Equatorial Subsurface Water (ESSW) mass represents salinity values higher than 33.8 $g\,kg^{-1}$. The ESSW was localized near the bottom of the Puyuhuapi Fjord and Jacaf Channel (Linford et al., 2023).

The long-term seasonal means were calculated using the Data-Interpolating Variational Analysis (DIVA) gridding software developed by the University of Liège (http://modb.oce.ulg.ac.be/mediawiki/index.php/DIVA, last access: 12 November 2023). The DIVA software was used to analyze and interpolate datasets via an optimal interpolation method, which considers the coastline and bathymetry of the study area; the calculations were executed on a finite-element mesh adapted to the study area domains (Troupin et al., 2010). Additionally, the DIVA results were graphically displayed using the Ocean Data View software (https://odv.awi.de, last access: 12 November 2023).

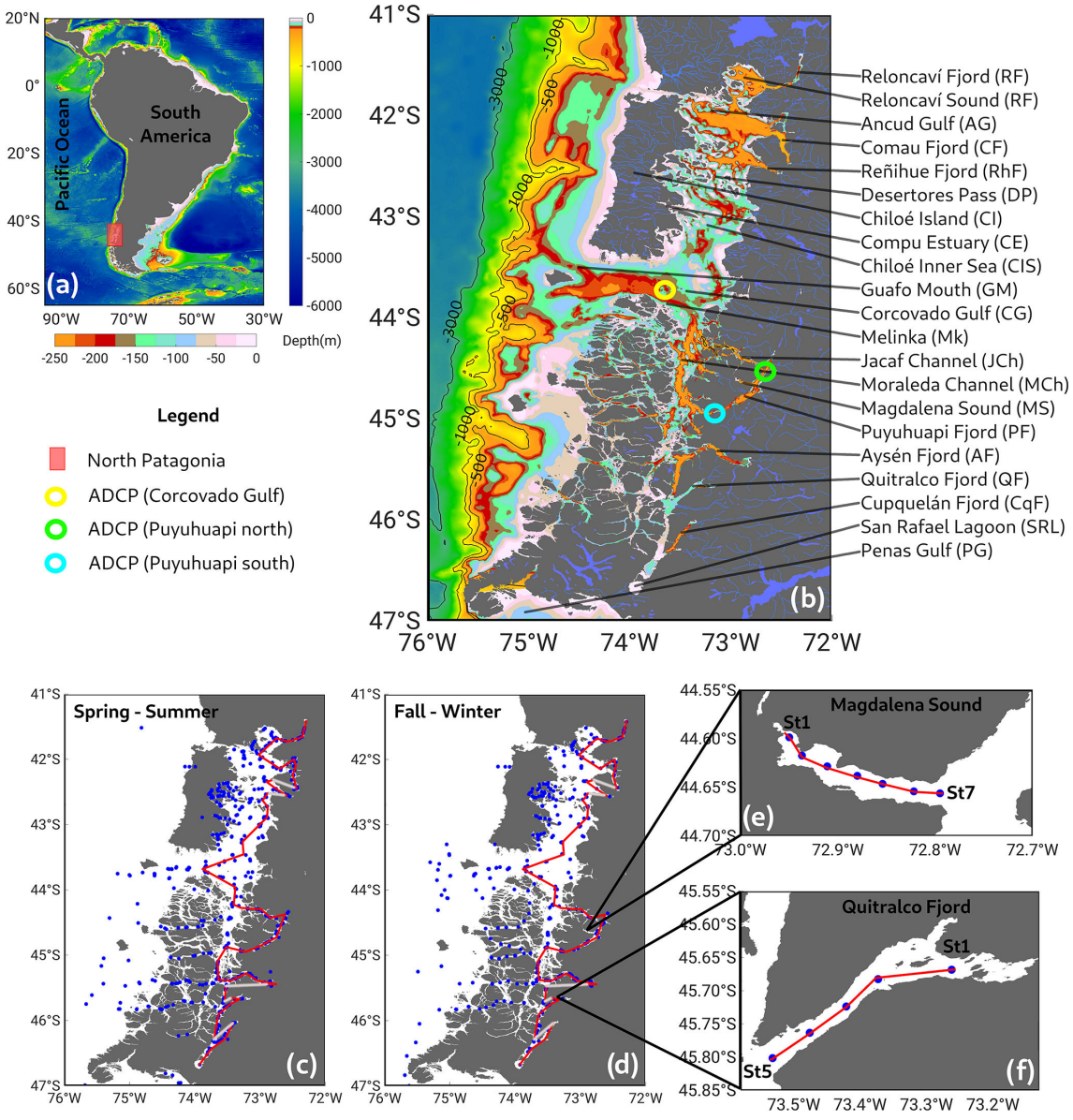



**Figure 1.** **(a)** Map showing the study area in the **(b)** northern region of the Patagonian fjords. Color bars represent bathymetric features from ETOPO2. **(c, d)** Sampling stations during the spring–summer and fall–winter seasons. Red lines in **(c)** and **(d)** represent along-fjord transects used to describe vertical features of hydrographic–chemical stations from Figs. 2, 4, and 5. Data were collected on sporadic cruises, from 1970–2021 (see Table 1). **(e, f)** Details of Magdalena Sound and the Quitralco Fjord sampling stations. Bathymetry was based on an SHOA (acronym for its Spanish name, Servicio Hidrográfico y Oceanográfico de la Armada de Chile) nautical chart from the Chilean Navy.

### 2.2 Primary production, community respiration, bacterial production, and phytoplankton community

During the spring–summer period of 2020–2021 and summer of 2022, nine in situ experiments were conducted to measure gross primary production (GPP) and community respiration (CR) in some fjords of northern Patagonia (Table 2). Water samples were obtained from three depths (2, 10, and 20 m depth) at each sampling station. GPP and CR rates were estimated from changes in DO concentrations observed during in situ incubation of light and dark bottles (Strickland, 1960). Water from the Niskin bottles was transferred into 125 mL (nominal volume) borosilicate bottles (gravimetrically calibrated) using a silicone tube. Five time-zero bottles, five light bottles, and five dark bottles were used at each incubation depth. Water samples were collected at dawn and incubated throughout the entire light period (approximately ∼ 8–9 h). Time-zero bottles were fixed at the beginning of each experiment, whereas the light and dark incubation bottles were at-

**Table 1.** Oceanographic campaigns carried out in Patagonian fjords and channels.

| Expeditions | Date (dd/mm/yyyy) | Season | Stations | Measurements |
|---|---|---|---|---|
| Hudson | 06/03–01/04/1970 | Summer | 112 | (Temperature, salinity)[a] + $O_2$(bottle Winkler) + nutrients ($PO_4$, $NO_3$, Si; bottle) |
| CIMAR-01 | 18/10–04/11/1995 | Spring | 99 | CTD + $O_2$(bottle Winkler) + nutrients ($PO_4$, $NO_3$, $NO_2$, Si; bottle) + pH(bottle) |
| CIMAR-04-I | 28/09–09/10/1998 | Spring | 31 | CTD + $O_2$(bottle Winkler) + nutrients ($PO_4$, $NO_3$, Si; bottle) |
| CIMAR-07-I | 07–21/07/2001 | Winter | 49 | CTD + $O_2$(bottle Winkler) |
| CIMAR-07-II | 13–25/11/2001 | Spring | 51 | CTD + $O_2$(bottle Winkler) + nutrients ($PO_4$, $NO_3$, Si; bottle) |
| CIMAR-08-I | 06–20/07/2002 | Winter | 51 | CTD + $O_2$(bottle Winkler) + nutrients ($PO_4$, $NO_3$, Si; bottle) |
| CIMAR-08-II | 16–24/11/2002 | Spring | 39 | CTD + $O_2$(bottle Winkler) + nutrients ($PO_4$, $NO_3$, Si; bottle) |
| CIMAR-09-I | 09–23/08/2003 | Winter | 58 | CTD + $O_2$(bottle Winkler) + nutrients ($PO_4$, $NO_3$, Si; bottle) |
| CIMAR-09-II | 07–20/11/2003 | Spring | 55 | CTD + $O_2$(bottle Winkler) + nutrients ($PO_4$, $NO_3$, Si; bottle) |
| CIMAR-10-I | 26/06–31/08/2004 | Winter | 49 | CTD + $O_2$(bottle Winkler) + nutrients ($PO_4$, $NO_3$, Si; bottle) |
| CIMAR-10-II | 12–23/11/2004 | Spring | 63 | CTD + $O_2$(bottle Winkler) + nutrients ($PO_4$, $NO_3$, Si; bottle) |
| CIMAR-11-I | 18–25/07/2005 | Winter | 78 | CTD + $O_2$(bottle Winkler) + nutrients ($PO_4$, $NO_3$, Si; bottle) |
| CIMAR-11-II | 11–21/11/2005 | Spring | 80 | CTD + $O_2$(bottle Winkler) + nutrients ($PO_4$, $NO_3$, Si; bottle) |
| CIMAR-12-I | 10–19/07/2006 | Winter | 32 | CTD + $O_2$(bottle Winkler) +nutrients ($PO_4$, $NO_3$, Si; bottle) |
| CIMAR-12-II | 04–12/11/2006 | Spring | 40 | CTD + $O_2$(bottle Winkler) + nutrients ($PO_4$, $NO_3$, Si; bottle) |
| CIMAR-13-I | 27/07–07/08/2007 | Winter | 42 | CTD + $O_2$(bottle Winkler) + nutrients ($PO_4$, $NO_3$, Si; bottle) |
| CIMAR-13-II | 02–12/11/2007 | Spring | 46 | CTD + $O_2$(bottle Winkler) + nutrients ($PO_4$, $NO_3$, Si; bottle) |
| CIMAR-17 | 17/10–14/11/2011 | Spring | 195 | CTD + $O_2$(bottle Winkler) + nutrients ($PO_4$, $NO_3$, Si; bottle) |
| CIMAR-18 | 01/06–04/07/2012 | Fall–winter | 98 | CTD + $O_2$(bottle Winkler) + nutrients ($PO_4$, $NO_3$, Si; bottle) |
| CIMAR-19 | 04–16/07/2013 | Winter | 70 | CTD + $O_2$(bottle Winkler) + nutrients ($PO_4$, $NO_3$, Si; bottle) |
| CHEPU-IFOP | 05–17/08/2017 | Winter | 22 | CTD + $O_2$(optic) |
| CIMAR-24 | 26/09–16/10/2018 | Spring | 37 | CTD + $O_2$(bottle Winkler) + nutrients ($NO_3$; bottle) |
| CHEPU-MR-I | 06–08/06/2018 | Fall | 12 | CTD + $O_2$(optic) |
| CHEPU-MR-II | 11/10/2018 | Spring | 2 | CTD + $O_2$(optic) |
| PN-I (IFOP) | 13–25/11/2020 | Spring | 32 | CTD + $O_2$(optic) + nutrients ($PO_4$, $NO_3$, $NO_2$, Si; bottle) + pH, Tur, Fluor[b] (optic) |
| PN-II (IFOP) | 24/02–04/03/2021 | Summer | 32 | CTD + $O_2$(optic) + nutrients ($PO_4$, $NO_3$, $NO_2$, Si; bottle) + pH, chl *a*, Tur, Fluor (optic) |
| PN-III (IFOP) | 28/07–10/08/2021 | Winter | 32 | CTD + $O_2$(optic) + nutrients ($PO_4$, $NO_3$, $NO_2$, Si; bottle) + pH, chl *a*, Tur, Fluor (optic) |
| Total of 1507 stations (593 stations during fall and winter and 914 stations during spring and summer seasons) | | | | |

[a] Temperature and salinity were measured with a reversing thermometer and inductive salinometer, respectively. [b] Tur and Fluor mean turbidity and fluorescence, respectively.

tached to the surface-tethered mooring system. The samples were incubated at the depths from which they were collected. Additionally, we presented GPP and CR values from February 2009 in Fig. 9, which have been previously published by Montero et al. (2011).

Dissolved oxygen concentrations were determined according to the Winkler method (Strickland and Parsons, 1968), using an automatic Metrohm burette (865 Dosimat plus) and automatic end-point detection (AULOX measurement system). Daily GPP and CR rates were calculated as follows: GPP = (mean [$O_2$] light bottles − mean [$O_2$] dark bottles); CR = (mean [$O_2$] time-zero bottles − mean [$O_2$] dark bottles). The GPP and CR values were converted from oxygen to carbon units using a conservative photosynthetic quotient of 1.25 (Williams and Robertson, 1991) and a respiratory quotient of 1.

A total of five bacterial production (BP) experiments were performed during the same period as mentioned above (Table 2). Experiments were conducted using the same water samples collected for the in situ GPP and CR incubation experiments. The BP estimates were based on the incorporation of leucine into proteins using the microcentrifugation method (Smith and Azam, 1992). Briefly, a blank and three samples (1.5 mL) were taken from each sampling depth and incubated with L-[3,4,5-$^3$H]-leucine (123.8 Ci mmol$^{-1}$, 40 nM final concentration) in the dark for 1 h. After incubation, samples were extracted with 100 % trichloroacetic acid (TCA), rinsed with 5 % TCA, and centrifuged at 13 500 rpm twice for 15 min before removal of the supernatant. The liquid scintillation cocktail Ecoscint (1 mL) (National Diagnostics) was added to each sample. The samples were counted for disintegrations per minute using a Packard (model 1600 TR) liquid scintillation counter. Discrete depth estimates of the GPP, CR, and BS rates were integrated to 20 m using the trapezoidal method.

For analyses of the phytoplankton community, water samples were collected from four discrete depths (2, 4, 10, and 20 m) using a 5 L Niskin bottle. Samples were stored in 120 mL clear plastic bottles and preserved in 1 % Lugol's iodine solution (alkaline). From each sample, a 10 mL subsample was placed in a sedimentation chamber and allowed to settle for 12 h (Utermöhl, 1958) prior to identification at 40× and 100× under an inverted microscope (Carl Zeiss, Axio Observer.A1). Finally, taxonomic descriptions from Tomas (1997) were used to identify phytoplankton composition.

### 2.3 Biogeochemical variables and analysis

Biogeochemical data were collected in November 2020 (Expedition PN-I (IFOP), Table 1). The water samples were obtained by filtering seawater collected (1–2 L) using a 25 mm

**Table 2.** Gross primary production (GPP), community respiration (CR), and bacterial secondary production (BSP) from in situ experiments in northern Patagonian fjords and channels.

| Fjord region | Date (mm/dd/yyyy) | Season | Measurements ($g\,C\,m^{-2}d^{-1}$) | | | |
|---|---|---|---|---|---|---|
| | | | GPP | CR | BSP | GPP : CR |
| Reloncaví* | 02/27/2009 | Summer | 3.83 | 3.31 | – | 1.16 |
| Compu | 10/03/2020 | Spring | 1.22 | 0.92 | 0.06 | 1.32 |
| Quitralco | 11/17/2020 | Spring | 1.41 | 2.66 | 0.05 | 0.53 |
| Camou | 12/12/2020 | Spring | 0.12 | 1.67 | 0.15 | 0.07 |
| Puyuhuapi | 01/21/2020 | Summer | 1.89 | 6.64 | 0.25 | 0.28 |
| Reloncaví | 01/14/2021 | Summer | 2.60 | 1.90 | 0.58 | 1.37 |
| Compu | 03/19/2022 | Summer | 1.25 | 0.76 | – | 1.64 |
| Quitralco | 02/28/2022 | Summer | 0.73 | 1.71 | – | 0.42 |
| Camou | 03/16/2022 | Summer | 0.56 | 1.12 | – | 0.50 |
| Puyuhuapi | 01/20/2022 | Summer | 2.18 | 2.55 | – | 0.85 |

* Data were taken from Montero et al. (2011).

diameter GF/F filter pre-combusted with a 0.7 µm pore diameter. Suspended particulate matter (SPM, $\mu g\,L^{-1}$), was determined by gravimetry using the weight difference between the dried filter and the same filter before filtration (Grasshoff et al., 2009). Particulate organic carbon (POC, $\mu mol\,L^{-1}$), total nitrogen (TN, $\mu mol\,L^{-1}$), stable carbon ($\delta^{13}C$, ‰), and nitrogen ($\delta^{15}N$, ‰) isotopes were obtained following the method described by Verardo et al. (1990), with modifications by Barrera et al. (2017) and Díaz et al. (2023), and measured at the Stable Isotope Facility at the Pontifical Catholic University of Chile using an elemental analyzer (EA; Flash 2000, Thermo Finnigan), interfaced to a continuous-flow isotope ratio mass spectrometer (IRMS; Delta V Advantage).

The stable carbon isotope composition of organic carbon ($\delta^{13}C$) can vary depending on its origin, with values ranging from −23 ‰ to −19 ‰ for carbon sources such as marine phytoplankton (Fry and Sherr, 1989; Harmelin-Vivien et al., 2008) and values closer to those of terrestrial organic matter (−30 ‰ to −26 ‰) for other sources (Fry and Sherr, 1989). By analyzing the carbon isotopic composition of organic carbon, it is possible to differentiate carbon between different sources and estimate their contributions. We calculated the relative importance of allochthonous and autochthonous organic matter with two-source endmember mixing models (Bianchi, 2007). The importance of autochthonous marine and allochthonous terrestrial fractions was calculated based on the following equation:

$$\%\,\mathrm{POC_{allo}} = \frac{\left(\delta^{13}C_s - \delta^{13}C_m\right)}{\left(\delta^{13}C_t - \delta^{13}C_m\right)} 100\,\%,$$

where $\delta^{13}C_s$ is the isotopic composition of a sample, $\delta^{13}C_m$ is the marine endmember from more oceanic stations (−13 447 ‰), and $\delta^{13}C_t$ terrestrial is the riverine endmember values for POC (−42 933 ‰) as proposed for this area by González et al. (2019). The resulting $\%\,\mathrm{POC_{allo}}$ represents the relative contribution of allochthonous (terrestrial) organic carbon to the overall organic carbon pool. Higher values indicate a more significant influence of terrestrial organic carbon, while lower values suggest a higher proportion of autochthonous (marine) organic carbon (González et al., 2019). The carbon : nitrogen ratio was also calculated as a proxy for the organic matter pool (Barrera et al., 2017).

Dissolved inorganic nutrients ($NO_3^-$, $NO_2^-$, $PO_4^{3-}$, and $Si(OH)_4$) were analyzed from 15 mL seawater samples, stored at −20 °C in HDPE bottles, using a Seal AA3 HR AutoAnalyzer according to the methodology described by Grasshoff et al. (1983) and standard methods for seawater analysis (Kattner and Becker, 1991). Chromophoric dissolved organic matter (CDOM) plays a crucial role in understanding the optical properties and biogeochemical processes in aquatic ecosystems (Stedmon and Nelson, 2015). It is an important component of dissolved organic matter (DOM) that absorbs light in the visible spectrum (ultraviolet and blue wavelengths) and fluoresces at longer wavelengths (Stedmon and Nelson, 2015). CDOM was determined by fluorometry using quinine sulfate dihydrate ($\mu g\,L^{-1}$) diluted in 0.1 N sulfuric acid at a specific wavelength as standard in a Turner Designs Trilogy fluorometer and CDOM module (Kim et al., 2018).

### 2.4 Satellite images

Sentinel-2 level-1 images were downloaded from the Copernicus Open Access Hub (https://scihub.copernicus.eu/, last access: November 2022) for specific dates and regions, as shown in Table 3. The chosen dates correspond to periods of high discharge of freshwater from the continent. Using ACOLITE v 20220222.0 (https://odnature.naturalsciences.be/remsem/software-and-data/acolite (last access: November 2022); Vanhellemont and Ruddick, 2018), we calculated the satellite suspended particulate matter (SSPM) following

**Table 3.** Dates and regions of the Sentinel-2 datasets analyzed.

| Date | Region |
|---|---|
| 17 March 2017 | Puyuhuapi Fjord |
| 9 May 2017 | Reloncaví Sound and Reloncaví Fjord |
| 6 April 2018 | Comau Fjord |
| 9 June 2022 | Quitralco Fjord |

Nechad et al. (2016). These data have a spatial resolution of 10 m and allow the resolution of the small-scale distribution of SSPM within the narrow channels and fjords of the region.

### 2.5 Marine current registered with ADCP

In the study region, three mooring systems were deployed in the Gulf of Corcovado and Puyuhuapi Fjord. In each mooring, a Teledyne RD Instruments (TRDI) and a Workhorse 300 kHz acoustic Doppler current profiler (ADCP) were installed with the transducers facing downward. The instruments were configured with 1 m cell size and 1 h ensembles. The moorings covered the period from January to December 2016, with the ADCP sensors moored between 40 and 100 m. The ADCP provides the current magnitude and direction (in Earth coordinates); thus, the current vector is decomposed into zonal ($u$) and meridional ($v$) components. The basic and standard protocol of quality control was applied to identify outliers and low-quality data following the methodology suggested by TRDI. To obtain the mean pattern of the zonal and meridional components of the currents, they were filtered using a low-pass cosine-Lanczos filter of 121 weight and 40 h half-power.

The currents were rotated following the main axis of the Guafo Channel and Puyuhuapi Fjord (Fig. 1), thus implying that in Guafo, currents were rotated 14° south of east, whereas in Puyuhuapi South currents were rotated 36° north of east and in Puyuhuapi North the axis was rotated 22° east of north. Following those rotations, the contours of the time series of the along-channel/fjord components are shown in Fig. 11.

### 2.6 Circulation model

To enhance our understanding of the DO dynamics' and physical factors, we utilized the MIKE 3 Wave FM hydrodynamic model. This model employs the finite-volume method to solve continuity, momentum, temperature, and salinity transport equations (DHI, 2019). This study focused on two high-resolution model domains: D1_Chiloé (41.3 to 43.7° S) and D2_Aysén (43.6 to 46.8° S) (Fig. S1a, b in the Supplement).

The D1_Chiloé and D2_Aysén models are part of the CHONOS initiative (Reche et al., 2021), available at http://chonos.ifop.cl/ (last access: September 2022). This platform offers an open-access oceanographic database, primarily tailored for environmental applications. Led by the Instituto de Fomento Pesquero (IFOP) and supported by the Undersecretariat for Fisheries and Aquaculture of the Chilean government, this system guides decisions concerning aquaculture in southern Chile. Moreover, this oceanographic database, grounded in the D1 and D2 domains, has been used in studies on harmful algal blooms (Mardones et al., 2021; Diaz et al., 2021), larval fish dispersion (Landaeta et al., 2023), and overarching marine circulation dynamics (Soto Riquelme et al., 2023; Pérez-Santos et al., 2019). The modeling process was conducted over 6 years, from 2016 to 2021. Owing to computational constraints, the development began with the D1_Chiloé domain, subsequently followed by D2_Aysén. Both domains employed a hydrostatic variant of the MIKE 3 model. Vertical discretization was implemented using hybrid coordinates, combining sigma- and $z$-level systems. The bathymetry was sourced from the nautical chart soundings provided by the Chilean Navy (http://www.shoa.cl/, last access: January 2022).

For atmospheric forcing, we used the Weather Research and Forecasting (WRF) model from the CHONOS initiative. This version provides a refined 3 km spatial resolution, tailored for the complex topography of the fjords. Its efficacy was previously described by Soto-Riquelme et al. (2023), who specifically evaluated its performance near the Guafo mouth, finding significant correlations with local meteorological stations, particularly in atmospheric pressure ($R = 0.99$) and wind ($R = 0.87$).

Freshwater sources were identified through the IFOP FLOW hydrological model, which employs precipitation and temperature series data from the CR2MET gridded product (http://www.cr2.cl/datos-productos-grillados/, last access: January 2022). Using these data, characterized by a spatial resolution of $5 \times 5$ km, enables the simulation of runoff and the calculation of daily discharge series. Based on IFOP FLOW estimates, the average annual freshwater discharge entering the D1_Chiloé domain during 2016–2021 was approximately $2545\,m^3\,s^{-1}$. Conversely, for the D2_Aysén domain, it was approximately $3126\,m^3\,s^{-1}$. The performance of the IFOP FLOW model at the gauged river stations of the Chilean water authority can be accessed at http://chonos.ifop.cl/flow/ (last access: July 2022) and in the Supplement.

Water levels at the open boundary were established using harmonic analysis (Pawlowicz et al., 2002), based on data from a regional barotropic model (Pinilla et al., 2012). Temperature and salinity boundary conditions were compiled from CTD profiles, collected during the CIMAR Fiordos oceanographic cruises (Guzmán and Silva, 2002; Valdenegro and Silva, 2003; Carrasco and Silva, 2010). Finally, boundary flow data were set to zero, ensuring an internal balance of current dynamics within the model domain both temporally and spatially. For an in-depth understanding of the configuration and model validation, kindly refer to the Supplement (Figs. S1–S8).

### 2.7 Flushing-time calculation

The MIKE 3 Wave FM hydrodynamic model data were used to calculate the flushing time via a conservative tracer. According to Takeoka (1984) and Monsen et al. (2002), flushing time is defined as the time required for the total mass of a material within a specific area such as a fjord, sound, or bay to be reduced by a factor of $e^{-1}$ (approximately 37 %) (Prandle, 1984). The interior and exterior of the area were assigned initial concentration values of 1 and 0, respectively. Throughout simulation, the original water mass of the basin was incrementally replaced with inputs from open boundaries and rivers. This variable symbolizes the proportion of original water in each element within the area of interest at a given time, facilitating the identification of less flushed areas within the modeled basins (Andrejev et al., 2004). The final values were derived from a temporal average from 2016 to 2021, and a vertical average was calculated from 50 m to the bottom, which represents the area that typically displays the lowest oxygen values. In the present study, the flushing time was implemented in the ECO Lab module of the MIKE 3 Wave FM for every fjord within D1_Chiloé and D2_Aysén.

## 3 Results

### 3.1 Long-term annual mean of hydrographic–chemical parameters

The long-term annual means include all datasets presented in Fig. 2a and b (location and detailed information in Fig. 1c and d and Table 1). This section scrutinizes the behavior of conservative temperature, absolute salinity, DO, and inorganic nutrients. The long-term seasonal mean of conservative temperature (CT) denoted warmer water in the northern region (41.5–43° S) during both seasons, between Desertores Pass and the Reloncaví Fjord (Fig. 2c–d). In contrast, cold waters were observed in the deep layer of the Puyuhuapi Fjord and Jacaf Channel, and the coldest water was registered in the San Rafael Lagoon. This location also had the lowest absolute salinity ($S_A = 15$ to 21 g kg$^{-1}$), indicating the presence of the EW owing to the contribution of the ice melting from the San Rafael Lagoon and river discharges (Fig. 2e–f). In this area, the EW moved from south to north and mixed with the SAAW, contributing to the origin of the MSAAW, as was observed in the vertical–horizontal salinity distribution. Moreover, the EW was also observed in the northern domain of the study area, especially at the surface layer in the Reloncaví system and the Comau and Reñihue fjords, contributing to the formation of the MSAAW. In this region, the origin of the EW was mainly attributed to the freshwater supply from river discharge. Therefore, we identified two different sources of the EW that led to the formation of the MSAAW: (1) the combination of ice melting from the San Rafael Lagoon with river discharge in the southern region and (2) the freshwater supply by river discharge in the northern region. Both sources contributed to the difference in conservative temperature observed in the MSAAW.

Finally, the ESSW enters the deep layer of the Guafo mouth, crosses the Gulf of Corcovado, and ends its travel at the deep layers of the Puyuhuapi Fjord and Jacaf Channel. During the fall–winter season, a slight reduction in ESSW distribution was observed (Fig. 2e–f). In the area contained by the ESSW, low-DO water (LDOW) and hypoxic waters were observed, but LDOW was registered at the Reloncaví Fjord, where the ESSW was not observed (Fig. 2g–h).

In general, the Chiloé inner sea showed a homogenized water column, during the fall–winter seasons, in which high DO values (267–312 µmol L$^{-1}$) and oversaturated waters (DO saturation > 100 %) were registered. In addition, high DO records were measured in the San Rafael Lagoon, between the Aysén and Puyuhuapi fjords, and in the Gulf of Corcovado (Fig. 2g–h). Furthermore, a larger area with hypoxic conditions and LDOW was recorded during the spring–summer seasons (Fig. 2g–h) compared to the fall–winter period. (Fig. 2g–h).

The quantification of water masses through a $T$–$S$ diagram (Fig. 3) highlights the dominance of the MSAAW, with proportions of 60.96 % and 54.67 % during the spring–summer and fall–winter seasons, respectively. Following closely, the SAAW was the second most dominant water mass, with proportions of 15.25 % and 22.64 %. The EW came next, and finally, the ESSW displayed the smallest proportion, with values of 10.77 % and 11.15 %. It is worth noting that the ESSW was characterized by cold, salty, and poor DO content in comparison to the EW, MSAAW, and SAAW, as detailed in Table 4.

As shown in Fig. 2, the Puyuhuapi Fjord and Jacaf Channel were regions where high-salinity waters and hypoxic LDOW were registered. In addition, a high concentration of inorganic nutrients was observed in the subsurface layer at depths greater than 50 m (Fig. 4). In the Puyuhuapi Fjord and the Jacaf Channel, between 100–300 m depth, nitrate (Fig. 4a), phosphate (Fig. 4c), and silicic acid (Fig. 4e) range from 25–30, 2–3, and 30–50 µM, respectively. A second area with high inorganic nutrients was detected in the Reloncaví system, in which the highest absolute values of surface silicic acid were registered during the fall–winter season (e.g., 210 µM). Comparing seasonal concentrations, the fall–winter season showed the highest abundance in the water column. However, the absolute maximum nitrate (Fig. 4b), phosphate (Fig. 4d), and silicic acid (Fig. 4f) values were recorded in the subsurface layer during the spring and summer seasons.

The calculation of the Brunt–Väisälä frequency (BVF), a variable used to identify mixed/stratified regions, evidenced a permanent mixing of the water column in the Chiloé inner sea (BVF < 10 cycles h$^{-1}$) (Fig. 5a–b). Furthermore, the homogenization of physical (e.g., conservative temperature and absolute salinity) and chemical (e.g., DO oxygen and inorganic nutrients) variables was observed in these

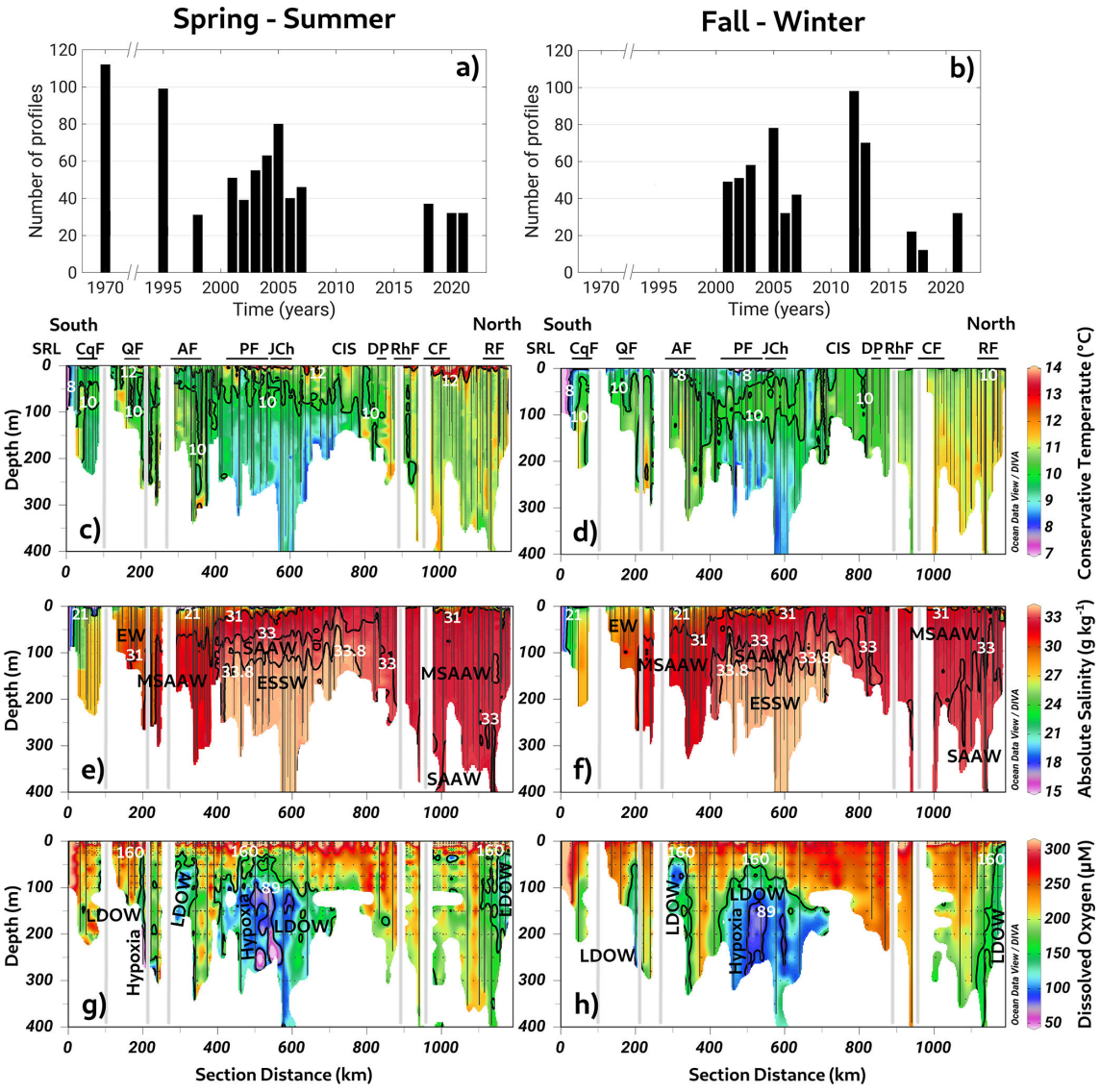



**Figure 2.** **(a, b)** Time series of conductivity, temperature, and depth (CTD) profiles used to compute seasonal averages. Long-term seasonal means of **(c–d)** conservative temperature, **(e–f)** absolute salinity, and **(g–h)** dissolved oxygen collected along a vertical section in the northern Patagonian fjords during the fall–winter and spring–summer seasons. See Fig. 1b for the abbreviations in **(c)** and **(d)**. **(c–h)** Figure credit goes to Reiner Schlitzer, Ocean Data View, https://odv.awi.de/ (last access: September 2023) (2023).

**Table 4.** Statistical characteristics of the water masses identified in the northern Patagonian fjords.

| Salinity criteria (Sievers and Silva, 2008) | | Spring–summer campaigns | | | | Fall–winter campaigns | | | |
|---|---|---|---|---|---|---|---|---|---|
| Water masses | Salinity range ($g\,kg^{-1}$) | Water masses (%) | Mean CT ± SD* (°C) | Mean $S_A$ ± SD ($g\,kg^{-1}$) | Mean DO ± SD ($\mu mol\,L^{-1}$) | Water masses (%) | Mean CT ± SD (°C) | Mean $S_A$ ± SD ($g\,kg^{-1}$) | Mean DO ± SD ($\mu mol\,L^{-1}$) |
| EW | 0–31 | 12.64 | $10.29 \pm 1.1$ | $27.92 \pm 4.7$ | $245.25 \pm 65.8$ | 11.92 | $9.70 \pm 0.8$ | $28.75 \pm 3.4$ | $238.02 \pm 56.8$ |
| MSAAW | 31–33 | 60.96 | $10.64 \pm 0.5$ | $32.44 \pm 0.5$ | $197.11 \pm 46.2$ | 54.67 | $10.55 \pm 0.6$ | $32.34 \pm 0.5$ | $231.82 \pm 37.6$ |
| SAAW | 33–33.8 | 15.25 | $10.49 \pm 0.6$ | $33.25 \pm 0.2$ | $196.03 \pm 41.9$ | 22.64 | $10.85 \pm 0.6$ | $33.19 \pm 0.2$ | $208.34 \pm 46.1$ |
| ESSW | 33.8 > | 11.15 | $9.12 \pm 0.4$ | $34.11 \pm 0.1$ | $109.57 \pm 32.6$ | 10.77 | $9.27 \pm 0.5$ | $34.13 \pm 0.1$ | $114.77 \pm 36.0$ |

* SD: standard deviation.

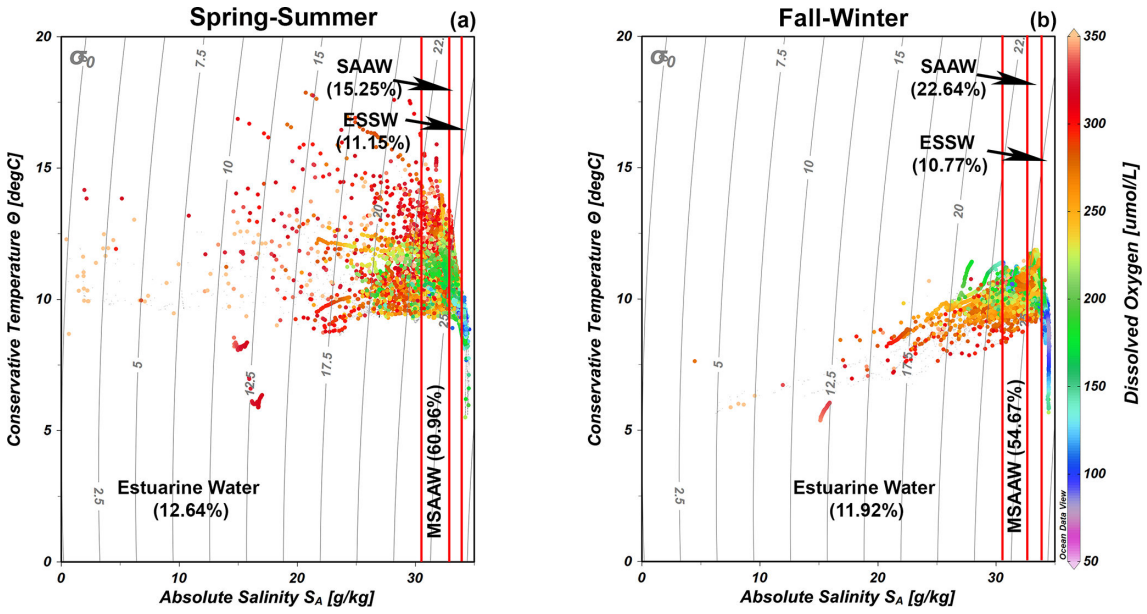



**Figure 3.** Temperature–salinity ($T$–$S$) diagrams with dissolved oxygen records showing the representation of water masses identified during the **(a)** spring–summer and **(b)** fall–winter seasons in the northern Patagonian fjords. The dataset utilized in the $T$–$S$ diagrams is described in Table 1. Figure credit goes to Reiner Schlitzer, Ocean Data View, https://odv.awi.de/ (last access: September 2023) (2023).

regions. In contrast, stratified water (between 2 and 10 m depth) was detected during spring–summer inside the fjords, e.g., Cupquelán, Quitralco, Aysén, Puyuhuapi, Comau, and Reloncaví, showing values of BVF $> 50$ cycles h$^{-1}$ that coincided with the lower salinity (Fig. 5a). The main drivers of the stratification in the northern Patagonian fjords depended on the freshwater supply by rivers and precipitation affecting the surface. The highest river flow relies on the melting of ice that occurs during the spring, but during the fall and winter, river flow is also increased due to the precipitation regime. Additionally, stratification was enhanced in summer because of the increase in solar radiation, making the spring–summer season the period where the absolute maximum stratification was registered (e.g., $\sim 100$ cycles h$^{-1}$) (Fig. 5a).

### 3.2 DO and chlorophyll-*a* features from sporadic oceanographic cruises

The analysis of hypoxia and LDOW conditions in the northern Patagonian fjord system highlighted the presence of two areas with waterbodies with these characteristics: the Puyuhuapi–Jacaf and Reloncaví regions. Moreover, Magdalena Sound (44.6° S, 72.9° W), located between the Puyuhuapi Fjord and the Jacaf Channel (Fig. 1), showed the shallowest hypoxia over the entire area of the northern Patagonian fjords. At this location, a 30 % DO saturation isoline was observed at a depth of 70 m, with the LDOW reaching a depth of approximately 20 m (Fig. 6a–c). Additionally, the lowest DO values of the northern Patagonian fjord system (9.36 µmol L$^{-1}$ and 1.6 % oxygen saturation) were recorded at the deepest layer ($\sim 200$ m) of the Quitralco Fjord (45.7° S, 73.3° W) (Fig. 6d–f).

The chlorophyll-*a* (chl-*a*) data collected during two oceanographic campaigns (Fig. 7a) denoted high concentrations of chl *a* in the Reloncaví Fjord, the Puyuhuapi Fjord, and the Jacaf Channel (Fig. 7b, c) where LDOW and hypoxia conditions were registered. The chl-*a* values observed during the winter season in the Reloncaví Fjord were exceptionally high (32.8 mg m$^{-3}$) and are discussed in Sect. 4. Regardless, in general, the winter season of August 2021 showed a lack of chl *a* in the southern part of the study area (Fig. 7c). The vertical distribution of the chl-*a* data described earlier was obtained through a statistical analysis between the fluorescence data from CTD casts (every 1 m depth) and the in situ chl-*a* samples from discrete levels (i.e., 0, 5, 10, 15, 25, and 50 m) (Fig. 7d–e).

### 3.3 Rates of primary production, community respiration, and bacterial production

The GPP and CR estimates obtained in our sampling agreed well with measurements reported in previous studies for the Patagonian fjords during the productive period (Iriarte et al., 2007; Montero et al., 2011, 2017b). The GPP and CR rates showed a weak coupling, with most experiments indicating that less oxygen is produced than is consumed (Fig. 8a). Thus, most fjords exhibited heterotrophic metabolism (GPP : CR $< 1$) in the surface layer (0–20 m) during the study period (Fig. 8b). The highest rates of GPP in terms of oxygen (18.6 to 41.02 mmol $O_2$ m$^{-3}$ d$^{-1}$) were

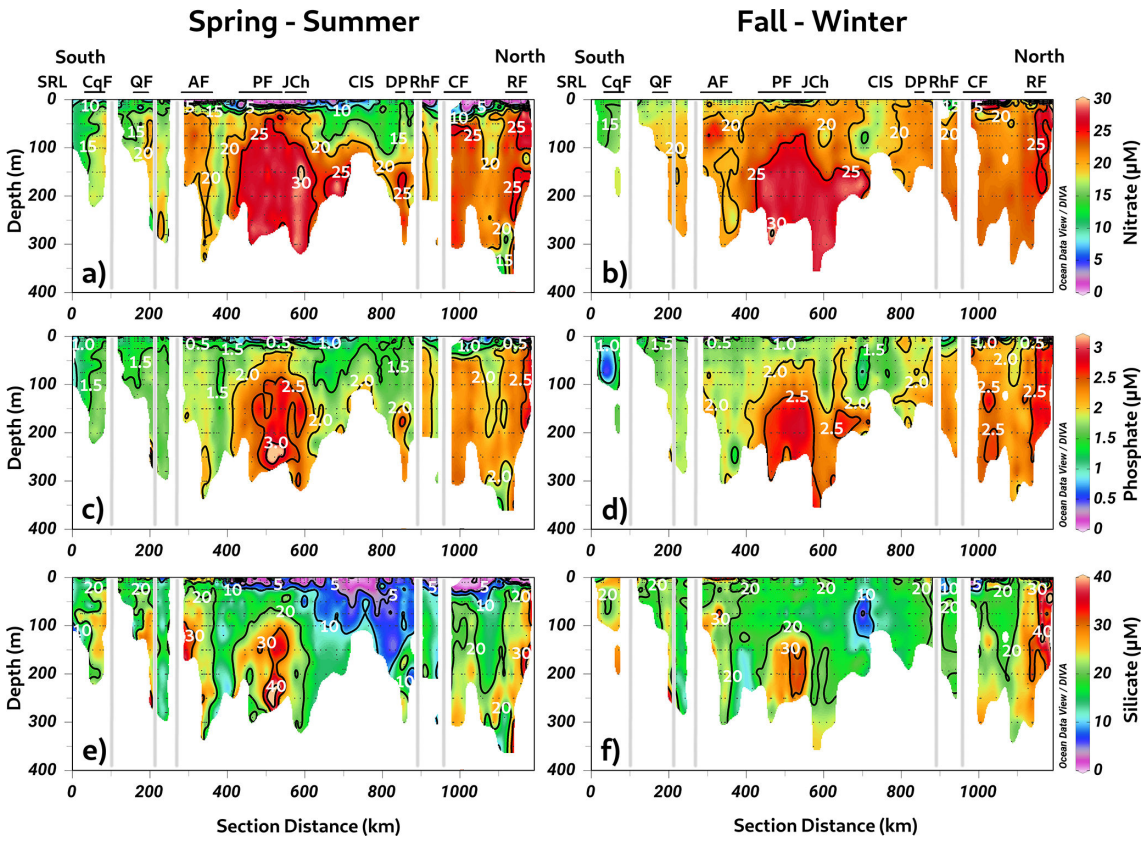



**Figure 4.** Long-term seasonal mean of inorganic nutrients. **(a, b)** Nitrate, **(c, d)** phosphate, and **(e, f)** silicate collected along a vertical section in the northern Patagonian fjord system during the fall–winter and spring–summer seasons. Figure credit goes to Reiner Schlitzer, Ocean Data View, https://odv.awi.de/ (last access: September 2023) (2023).

mainly recorded in the upper 5 m of the water column, whereas the lowest values (0 to 17.6 mmol $O_2$ $m^{-3}$ $d^{-1}$) were observed between 10 and 20 m depth (Fig. 8c to j). CR rates did not show a definite vertical pattern, registering their highest (23.3 to 76.3 mmol $O_2$ $m^{-3}$ $d^{-1}$) and lowest (0 to 12.3 mmol $O_2$ $m^{-3}$ $d^{-1}$) values throughout the water column (0–20 m) (Fig. 8c–j).

Throughout the study period in different fjords, integrated GPP and CR rates (down to 20 m) ranged from 0.1–2.6 and from 0.8–6.6 g C $m^{-2}$ $d^{-1}$, respectively (Fig. 9, Table 2). Neither rate showed significant differences ($p > 0.05$) between spring–summer 2020–2021 (Fig. 9a) and the summer of 2022 (Fig. 9b). Although there were no significant differences ($p > 0.05$) between GPP values recorded from different fjords in both study periods (Fig. 9a–b), the Comau Fjord showed the lowest rates of GPP (0.1 to 0.6 g C $m^{-2}$ $d^{-1}$), whereas Puyuhuapi and Reloncaví fjords showed the highest values (1.9 to 2.6 g C $m^{-2}$ $d^{-1}$). In the case of CR, the highest rates were recorded in the Puyuhuapi Fjord (2.2 to 6.6 g C $m^{-2}$ $d^{-1}$) and the lowest in the Comau Fjord (0.8 to 0.9 g C $m^{-2}$ $d^{-1}$) (Fig. 9a, b). The phytoplankton composition in the study area showed a similar pattern to the GPP values, highlighting maximum abundances on the surface and minimal abundances at a depth of 20 m (data not shown). In addition, the Comau Fjord showed the lowest abundances ($66 \times 10^3$ cells $L^{-1}$), whereas the Reloncaví Fjord showed the highest concentrations of phytoplankton ($1227 \times 10^3$ cells $L^{-1}$).

Estimated rates of BSP ranged between 0.05 and 0.6 g C $m^{-2}$ $d^{-1}$ within the study area and were positively and significantly correlated with GPP values (Fig. 9, Table 2). The percentage of GPP utilized by bacteria ranged from 3 % to 56 %, except in the Comau Fjord, where a higher utilization percentage (151 %) was recorded, suggesting that more organic carbon is consumed than is produced locally.

### 3.4 Satellite image of organic matter supply to fjords

Satellite images show that freshwater inputs into the sea were accompanied by large quantities of suspended particles (Fig. 10), possibly acting as a source of allochthonous organic matter, favoring the heterotrophic metabolism reported in the previous section. On 9 May 2017, a large amount of suspended matter flowed into Reloncaví Sound from its fjord, mainly dominated by three rivers: the Petrohué, Cochamó, and Puelo (Fig. 10b). In the southeastern part of Reloncaví

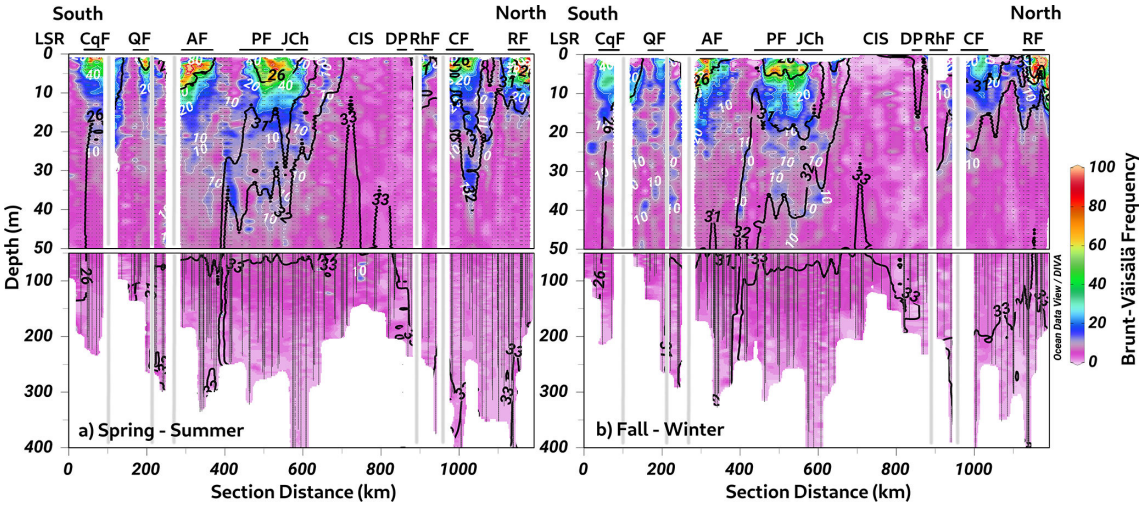



**Figure 5.** The long-term seasonal mean of Brunt–Väisälä frequency along a vertical section in the northern Patagonian fjords during the **(a)** spring–summer and **(b)** fall–winter seasons. The white and black contour lines denote the Brunt–Väisälä and absolute salinity values. Figure credit goes to Reiner Schlitzer, Ocean Data View, https://odv.awi.de/ (last access: September 2023) (2023).

Sound, the observed high concentration of suspended particles was accompanied by the presence of a diatom bloom (evidenced by greenish waters on the true-color images in the southeastern part of Reloncaví Sound), mainly formed by *Skeletonema costatum*, which attained concentrations of more than $5 \times 10^6$ cells $L^{-1}$ within the fjord (Fig. S8). This bloom affected both the eastern part of Reloncaví Sound and the Reloncaví Fjord. The amount of suspended matter visible in the Sentinel-2 images was generally homogeneously high along the fjords, e.g., on 9 June 2022, in the Quitralco Fjord (Fig. 10c), and 9 May 2017, in Reloncaví (Fig. 10b). However, heterogeneous distribution can also be found (e.g., on 6 April 2018 in the Comau Fjord, Fig. 10d), suggesting the influence of suspended particles within the fjord, in turn suggesting the influence of the currents in the distribution of waters rich in sediment. On this date, waters flowing from the river Blanco in the northern part of the fjord's mouth were whitish. Water flowing into this fjord from the south, principally from the Lloncochaigua and Vodudahue rivers, has a more brownish color.

At the Quitralco Fjord (Fig. 10c), SSPM from Río de los Huemules (at 45.54° S, 73.30° E; the brown riverbed is clearly visible in the natural color insert) appeared to propagate within the fjord, affecting the water clarity along the entire fjord. Inspection on other dates (not shown) revealed high variability in the direction of the river outflow, sometimes entering the fjord (and staying there for extended periods) and sometimes being directed towards the south. Finally, the Puyuhuapi Fjord also registered a high signal from SSPM due to river discharge; for example, the Ventisquero River was located at the fjord head (Fig. 10e). Other rivers, such as the Cisnes, Marta, and Uspallante, could also influence the supply of allochthonous organic matter to the Puyuhuapi Fjord, contributing to a decrease in DO and hypoxia. However, the cloud cover does not allow for better satellite images.

### 3.5 Biogeochemical variables

We observed different signals of SPM (Fig. 11b) along a latitudinal transect conducted from north to south in the northern Patagonian fjords (Fig. 11a). Specifically, significant increases in SPM were registered in the Cupquelán Fjord ($\sim 7\,mg\,L^{-1}$) and at the surface layer of the mouths of the Comau Fjord ($\sim 6\,mg\,L^{-1}$). Furthermore, smaller areas with values of SPM $> 3\,mg\,L^{-1}$ were found at the subsurface layer of the Quitralco and Aysén fjords. In the northern region, within the Chiloé inner sea and the subsurface layer of the Comau and Reloncaví fjords, SPM values were minimal.

The percentage of allochthonous organic carbon (% $POC_{allo}$) exhibited an irregular distribution in the southern area, with surface minimums under 30 % at the mouths of the Quitralco, Aysén, and Puyuhuapi fjords (Fig. 11c). In the northern area, the Comau Fjord and Reloncaví Sound presented low % $POC_{allo}$ values. Along the water column, % $POC_{allo}$ appeared to increase with depth, reaching values of approximately 70 %, except in the inner sea of Chiloé, where it was under 50 %. The C : N ratio exhibited a discernible reduction with increasing depth along the water column in the broader study area, encompassing the Chiloé inner sea region and extending to the Reloncaví Fjord. Although a similar C : N ratio trend was observed in both Chiloé and Reloncaví, the predominant feature is not a uniform "depth-dependent decrease" but rather an overall modest vertical gradient, ranging from 6–9. Furthermore, despite their comparably low C : N ratios, Chiloé and

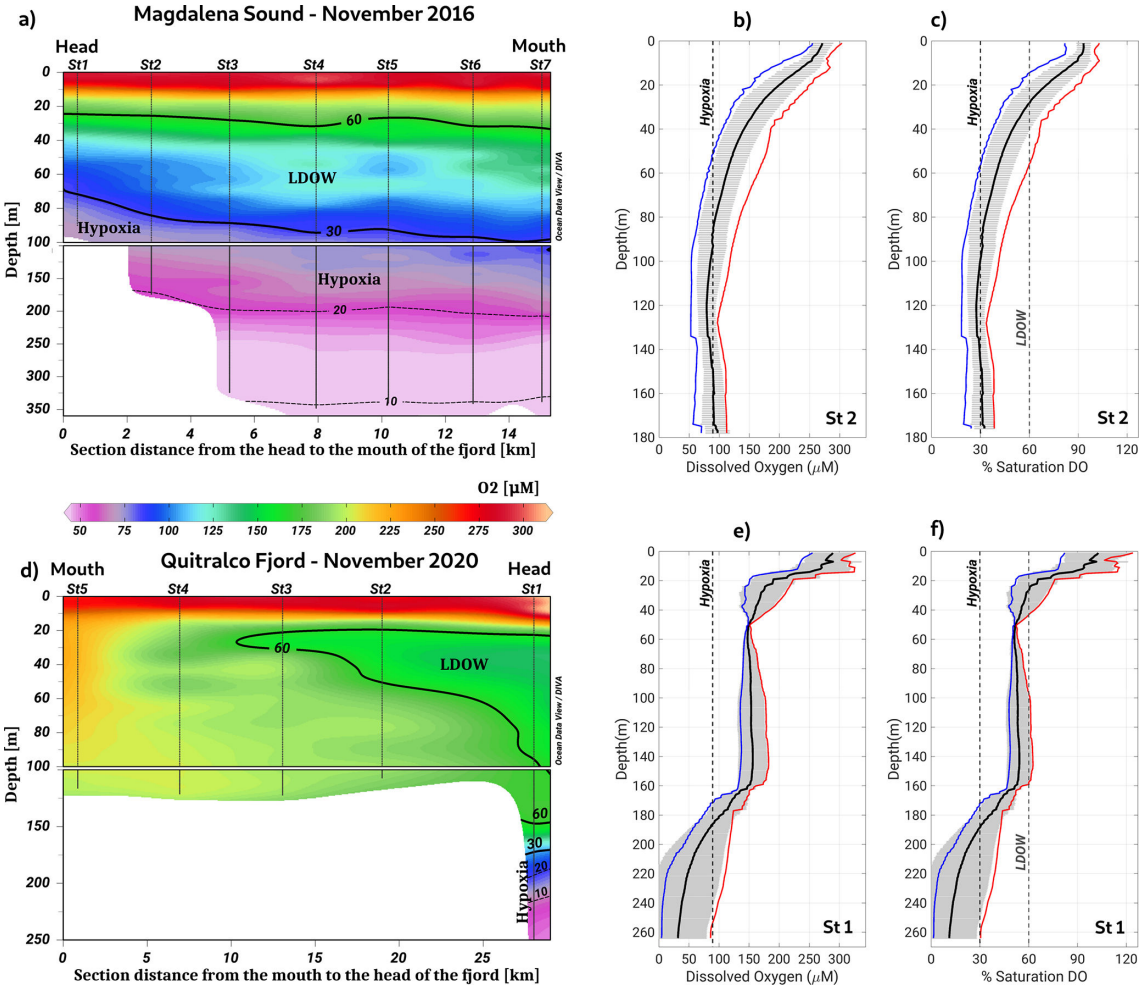



**Figure 6.** Vertical section of dissolved oxygen along **(a–c)** Magdalena Sound and **(d–f)** the Quitralco Fjord during November 2016 and November 2020, respectively. In **(b)**, **(c)**, **(e)**, and **(f)**, red, black, and blue lines represent the absolute maximum, average, and minimum values of DO, respectively. Gray shading shows the standard deviations calculated using 16 profiles for Magdalena Sound and 3 profiles for the Quitralco Fjord. **(a, d)** Figure credit goes to Reiner Schlitzer, Ocean Data View, https://odv.awi.de/ (last access: September 2023) (2023).

Reloncaví have differing CDOM concentrations, isotopic compositions, and POC allocations. Specifically, the Chiloé inner sea and Reloncaví Fjord exhibit analogous patterns of minimum C : N ratios (6–9). In addition, the subsurface regions of the Puyuhuapi and Aysén fjords register absolute maximum values (C : N > 14), as depicted in Fig. 11d.

The isotopic signal of the carbon ($\delta^{13}$C) increased in the same sites where % $POC_{allo}$ decreased, with values ranging from −25 ‰ to −15 ‰ (Fig. 11e). At the subsurface layer, the $\delta^{13}$C signal became lighter than that at the surface. An exception was observed in the Chiloé inner sea and the transition zone between the Aysén Fjord and San Rafael Lagoon, where the C : N ratio coincidentally decreased. In the region extending from the southern Chiloé inner sea to the Aysén Fjord, elevated levels of the isotopic signal of nitrogen ($\delta^{15}$N) enrichment were observed, primarily at the surface and subsurface levels (Fig. 11f). Notably, there was a significant increase in nitrogen values, with some exceeding 9 %; particularly, in the Chiloé inner sea, the enrichment extended to depths of 150–200 m.

The first CDOM observations in the Patagonian fjords denoted high concentrations throughout the water columns in the north area, spanning the Chiloé inner sea to the Reloncaví system (Fig. 11g). Conversely, in the southern area, CDOM concentrations declined, with minimum values as low as 20 µg $L^{-1}$ of specific UV absorbance between the Jacaf Channel and San Rafael Lagoon, but the absolute minimum was registered in the Comau Fjord. Despite this overall decrease, localized increases in CDOM concentrations were identified in certain fjords, such as Aysén, Quitralco, and the San Rafael Lagoon. These subsurface concentration spikes highlight the spatial variability in the CDOM distribution within the fjord system. Moreover, these findings provide valuable insights into the spatial distribution patterns of

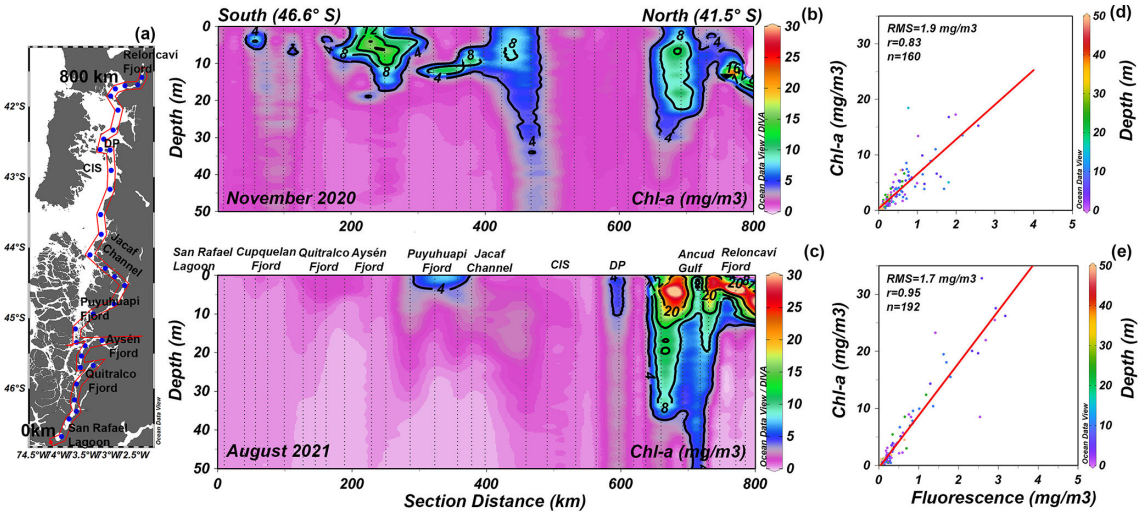



**Figure 7. (a)** Distribution map of the stations. Vertical distribution of chlorophyll *a* (chl *a*) during **(b)** November 2020 and **(c)** August 2021 in the northern Patagonian fjords. **(d, e)** Statistical relationship between the fluorescence data from CTD and in situ chl-*a* samples. In **(d)** and **(e)** RMS is the root mean square, *n* is the number of data points used to obtain the *R* values, and red lines represent the lineal tendency fit. In **(b)** and **(c)** CIS is the Chiloé inner sea and DP is Desertores Pass. Figure credit goes to Reiner Schlitzer, Ocean Data View, https://odv.awi.de/ (last access: September 2023) (2023).

CDOM in the Patagonian fjords, indicating higher concentrations in the northern region and a decline towards the southern end of the study area. The localized increases in CDOM concentrations in specific fjords suggest the influence of local processes or inputs contributing to the observed spatial heterogeneity.

### 3.6 Circulation regime from ADCP measurements

The low-frequency deep circulation (> 40 m depth) in the mooring of the Gulf of Corcovado showed a marked east–west direction in the along-channel current amplitude (Fig. 12b). The Corcovado currents were dominated by an eastward flow with a maximum intensity of approximately 30 cm $s^{-1}$ (Fig. 12a–b), whereas at the mouth of the Puyuhuapi Fjord (Fig. 12c–d), the maximum current was approximately 10 cm $s^{-1}$.

The Corcovado currents showed a marked pattern in the 40–70 m layer, which was dominated by westward currents, and short-duration events of approximately 20 cm $s^{-1}$ were observed throughout the entire time series. This intense westward flow seems to be associated with the austral spring–summer seasons (January–March and November–December 2016); however, a weak ($\sim$ 5 cm $s^{-1}$) and longer (July–October 2016) westward flow was observed during the austral fall–winter period. In the layer between 70 and 130 m, eastward (and intense) currents dominated, and there were periods of 1 to 2 months with eastward flow during March–April, May–July, and September–December 2016 with currents > 20 cm $s^{-1}$. The layer between 100 and 130 m showed maximum currents of approximately 40 cm $s^{-1}$ at the end of October 2016 (Fig. 12a).

Puyuhuapi Fjord currents were obtained at the southern mouth (southern Puyuhuapi, Fig. 12c–d) and middle fjord (northern Puyuhuapi, Fig. 12e–f. At the mouth of the fjord, low-frequency currents showed short pulses that covered most of the 70–160 m layer; typically, those pulses were eastward without an evident seasonal pattern. A unique low-frequency westward event was observed in mid-April 2016, which was also present in the Gulf of Corcovado. In general, the currents in southern Puyuhuapi were weak (< 10 cm $s^{-1}$); however, during September and October 2016, eastward events of 20 cm $s^{-1}$ were observed. In northern Puyuhuapi, most currents were weak (< 10 cm $s^{-1}$) without a temporally or spatially evident pattern, and the flow tended to be northward and intensified between May and September 2016.

### 3.7 Circulation regimen oceanographic model

Deep subtidal currents (average of 50–300 m) over the 3 years of simulation have a relatively large spatial variation (Fig. 13a–b). The model could correlate the most energetic zones in the outer channels with those of lower energy inside the fjords. In general, the exchanges between the fjords and ocean registered high average velocities, that is, the Guafo mouth, the Moraleda Channel, the Gulf of Corcovado, and Desertores Pass, with net current velocities ranging from 10 to 20 cm $s^{-1}$. In contrast, in the fjords, the average velocity of the deep flow was less than 5 cm $s^{-1}$. The predominant flow was generally towards the interior of the fjords (Fig. 13b).

The flushing/residence time calculated for each fjord showed that the sector towards the head of the Puyuhuapi

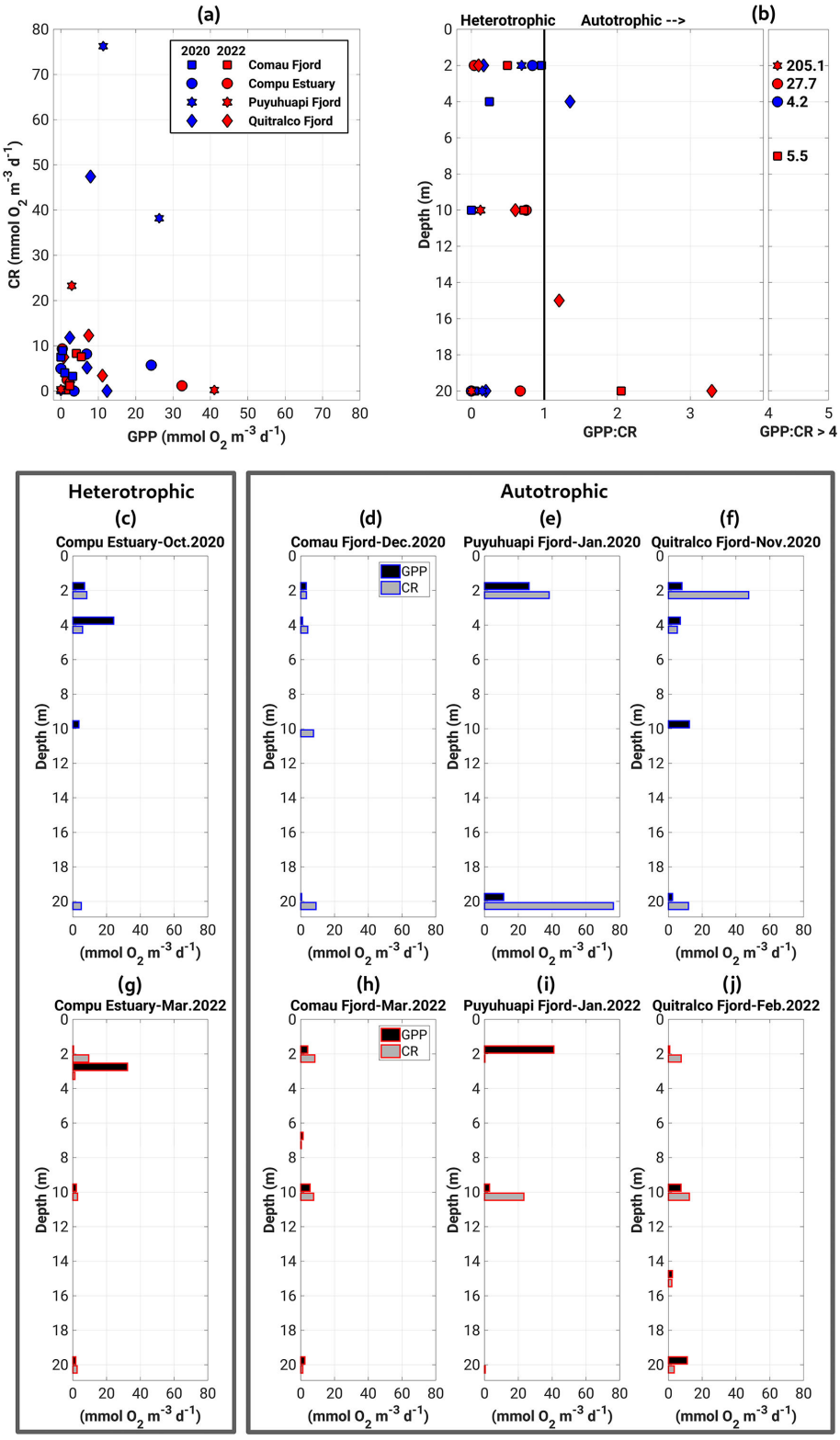



**Figure 8.** **(a)** Relationship and **(b)** vertical patterns of all datasets of the GPP and CR. Panels **(c)**–**(j)** represent the vertical distribution of GPP and CR obtained during experiments of primary production in **(c–f)** the spring–summer of 2020–2021 and **(g–j)** the summer of 2022. GPP: gross primary production; CR: community respiration.

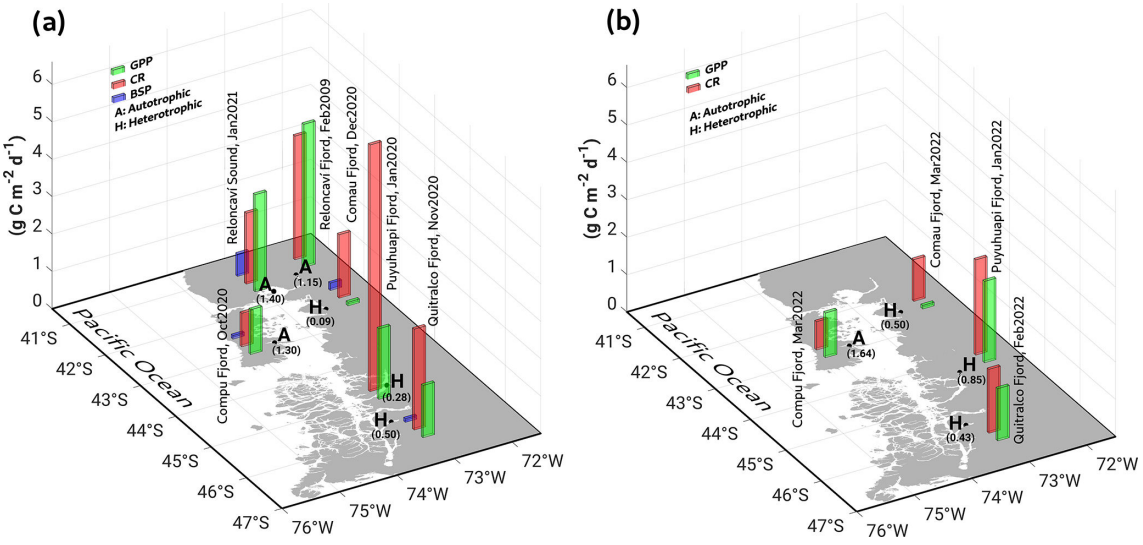



**Figure 9.** In situ measurements of primary production during **(a)** spring–summer of 2020–2021 and **(b)** summer of 2022, covering some fjords in the northern Patagonian fjord system. GPP: gross primary production; CR: community respiration; BSP: bacterial secondary production. Results shown from the Reloncaví Fjord in **(a)** were extracted from Montero et al. (2011).

Fjord registered the longest retention time (> 200 d). In comparison, the shortest times were found in Reloncaví Sound–the Reloncaví Fjord (60–90 d), except for the Reloncaví Fjord head, which reached values close to 100 d (Fig. 13c and d). The Comau Fjord showed relatively high values, which increased from mouth to head. In the central part of the Comau Fjord, the residence time ranged from 90 to 120 d, whereas at the fjord head, it ranged from 150 to 190 d. Meanwhile, the Aysén Fjord showed residence time values lower than 120 d, which were higher towards the fjord head, whereas the Quitralco Fjord had residence times of 150 d at the fjord head and 100 d at its central part. Finally, the Cupquelán Fjord exhibited greater homogeneity throughout the fjord, with relatively high values ranging from 120 to 150 d. The areas of longer residence time coincided with the region of LDOW and hypoxia (Fig. 13e–f).

## 4 Discussion

Oceanographic research in the Patagonian fjords started in 1995 with the CIMAR fjords project, supported by the Chilean Navy. As an oceanographic sampling strategy, Patagonia was divided into three zones, i.e., northern (41–47° S), central (47–53° S), and southern (53–55.8° S) Patagonia, and the frequency of the cruises was primarily seasonal (Sievers, 2008). Moreover, other oceanographic cruises, such as the Hudson expedition in 1970, occurred in this zone (Table 1). The data collected through the CIMAR projects allowed us to understand the main physical (water mass quantification) and chemical (e.g., dissolved oxygen and inorganic nutrients) processes impacting this fjord system, such as the hypoxic conditions due to the influence of the ESSW (Sievers, 2008; Sievers and Silva, 2008; Silva, 2008; Silva and Vargas, 2014; Schneider et al., 2014; Pérez-Santos et al., 2014). Furthermore, some studies about biological processes that include the consumption of DO, such as respiration and the remineralization of organic matter, have also contributed to our understanding of the processes that favor hypoxia and DO depletion (Montero et al., 2011, 2017a; Iriarte 2018). Additionally, the development of hydrodynamic models has helped to determine the areas where the water age was significantly high, for example, the Puyuhuapi Fjord (Pinilla et al., 2020), and where stronger mixing and stratification occurred (Ruiz et al., 2021). Our study scrutinized the natural processes contributing to the presence of water under hypoxic conditions and LDOW in the northern Patagonian fjords, as discussed in the next section.

### 4.1 Water mass properties and biogeochemical processes in northern Patagonian fjords

Recent and historical hydrographic data collected from the Patagonian fjords, especially in the northern area, have confirmed the presence of analogous water masses detected previously by the Hudson oceanographic cruise in 1970. The EW, MSAAW, SAAW, and ESSW were recorded from the surface layer to the bottom (to a depth of approximately 500 m) (Figs. 2 and 3). Similar patterns were recognized in terms of the vertical–horizontal distributions, highlighting the location of the salty–hypoxic waters/LDOW and nutrient-rich waters associated with the ESSW in the Jacaf Channel and Puyuhuapi Fjord (Figs. 2 and 4). This water mass enters Patagonia within the subsurface layers via the Guafo mouth and moves south throughout the Moraleda Channel to end at the Puyuhuapi Fjord and Jacaf Channel (Linford et al., 2023).

In contrast, the EW dominated in the southern area due to freshwater input from the San Rafael Lagoon and river discharge, which is characterized by oxygenated waters due to its high solubility and recent contact with the atmosphere. Finally, the SAAW and MSAAW covered the entire study area (Fig. 2), as reported by Sievers and Silva (2008), Schneider et al. (2014), Pérez-Santos et al. (2014), and Pinilla et al. (2020).

An absence of stratification was observed throughout the year in the Chiloé inner sea (Fig. 5). In this area, both physical and biogeochemical variables showed homogeneous values from the surface layer to the bottom (Figs. 2 and 4), indicating the presence of the MSAAW (originating from mixing the SAAW with the EW). Furthermore, the calculation of the buoyancy frequency and potential energy anomalies using the output from the oceanographic model demonstrated that more robust mixing occurred in the Chiloé inner sea (Ruiz et al., 2021). This explains the importance of this area for DO ventilation and redistribution in the northern Patagonian fjords.

Water masses in northern Patagonia have unique physicochemical properties (Sievers and Silva, 2008; Silva, 2008; Silva and Vargas, 2014; Schneider et al., 2014; Pérez-Santos et al., 2014). In the case of northern Patagonian fjords, the EW is rich in silicate (Fig. 4f) because of the riverine supply (Silva and Vargas, 2014), with characteristic high spatial variability in silicate at the surface layer that changes throughout the year due to the organisms' consumption (Montero et al., 2011), as observed in northern Patagonia, including the Chiloé inner sea (Fig. 4). Organic matter degradation processes occurred inside the fjords, mainly in terms of nitrogenous compounds being remineralized. These processes increase the nutrient pool that is originally transported by oceanic water and are responsible for the high accumulation of nitrate and phosphate registered in the subsurface layer of the Puyuhuapi Fjord and Jacaf Channel (Fig. 4).

Inside the fjords, where low salinity from high river discharge dominated, a persistent halocline–pycnocline–stratified water column developed; therefore, deep-water ventilation by vertical mixing and diffusion with the oxic surface layer was limited (Figs. 2–5). These conditions favored the occurrence of LDOW zones in the fjords, where stratification and particulate organic matter input were higher than at the mouths (Fig. 10). Thus, DO consumption was favored owing to organic matter degradation in the Reloncaví, Comau, Puyuhuapi, Aysén, and Quitralco fjords (Fig. 2), as has been reported for Piopiotahi / Milford Sound in New Zealand (Stanton, 1984), the Framvaren Fjord in Norway (Yao and Millero, 1995), the lower Saint Lawrence Estuary in Canada (Lefort, 2012), and Rivers Inlet in British Columbia (Jackson et al., 2022).

A latitudinal transect from north to south in the study area revealed distinct signals of SPM within the fjords. A noteworthy pattern of increased SPM levels below the surface was observed at the fjord mouths, particularly in the southern part of the study area (Fig. 11b). This finding suggests that the fjord mouth plays a crucial role in particulate organic matter accumulation, potentially originating from terrestrial sources. Furthermore, the high SPM values observed in the southern region indicate substantial contributions of allochthonous material, which may be influenced by factors such as river discharge, sediment resuspension, and glacial activity (Gonzalez et al., 2010). A more detailed analysis of SPM distribution revealed irregular patterns in the percentage of allochthonous organic matter (% $POC_{allo}$). At the mouths of the Quitralco, Aysén, and Puyuhuapi fjords, a surface minimum indicated relatively low terrestrial organic matter inputs as was reported by Gonzalez et al. (2010). The low-level input of organic matter could be attributed to limited river contributions or the autochthonous organic material production rate coinciding with nutrient depletion and increased DO (Holding et al., 2017).

In contrast, areas such as the Jacaf Channel and the Chiloé inner sea exhibited higher contributions of % $POC_{allo}$, indicating a more significant influence of allochthonous sources. Further, the increase in % $POC_{allo}$ with depth highlights the importance of vertical transport and sedimentation processes in determining the distribution of organic matter throughout the water column (Fig. 11c). Given the notable seasonality in carbon fluxes and fjord system dynamics, as highlighted by Gonzalez et al. (2010), the potential implications extend to the variability in trophic webs and carbon export. Recognizing that these effects are more autonomous from local primary production than open-ocean water systems is crucial. The seasonally driven variations in carbon fluxes can significantly influence the intricate interactions within trophic webs and contribute to fluctuations in carbon export processes within the fjord system. The C : N ratio exhibited spatial variability, with more homogeneous values in surface layers shallower than 50 m (Fig. 11d).

On average, the bulk particulate organic carbon and nitrogen concentrations maintained a C : N ratio of 8.5 : 1, exceeding the Redfield ratio of 6.6 : 1 typically observed in phytoplankton biomass within the marine realm (Redfield, 1958). Notably, the southern region exhibited higher C : N ratios, coinciding with areas with elevated SPM levels and increased % $POC_{allo}$. While the intuitively higher C : N ratio could be attributed to terrestrial sources with a higher carbon-to-nitrogen content, a more plausible explanation could be the increasing trend of the C : N ratio with depth and elevated particulate organic carbon ($POC_{allo}$) or a combination of both. The observed C : N ratios suggest the influence of microbial remineralization processes and the preferential removal of nitrogen-rich organic matter (Taucher et al., 2020), potentially resulting in a lower $POC_{allo}$ signal. The increase in the C : N ratio with depth likely reflects the consumption and degradation of sinking particles by zooplankton and heterotrophic bacteria, resulting in the preferential remineralization of nitrogen (Fig. 3) over carbon and the subsequent

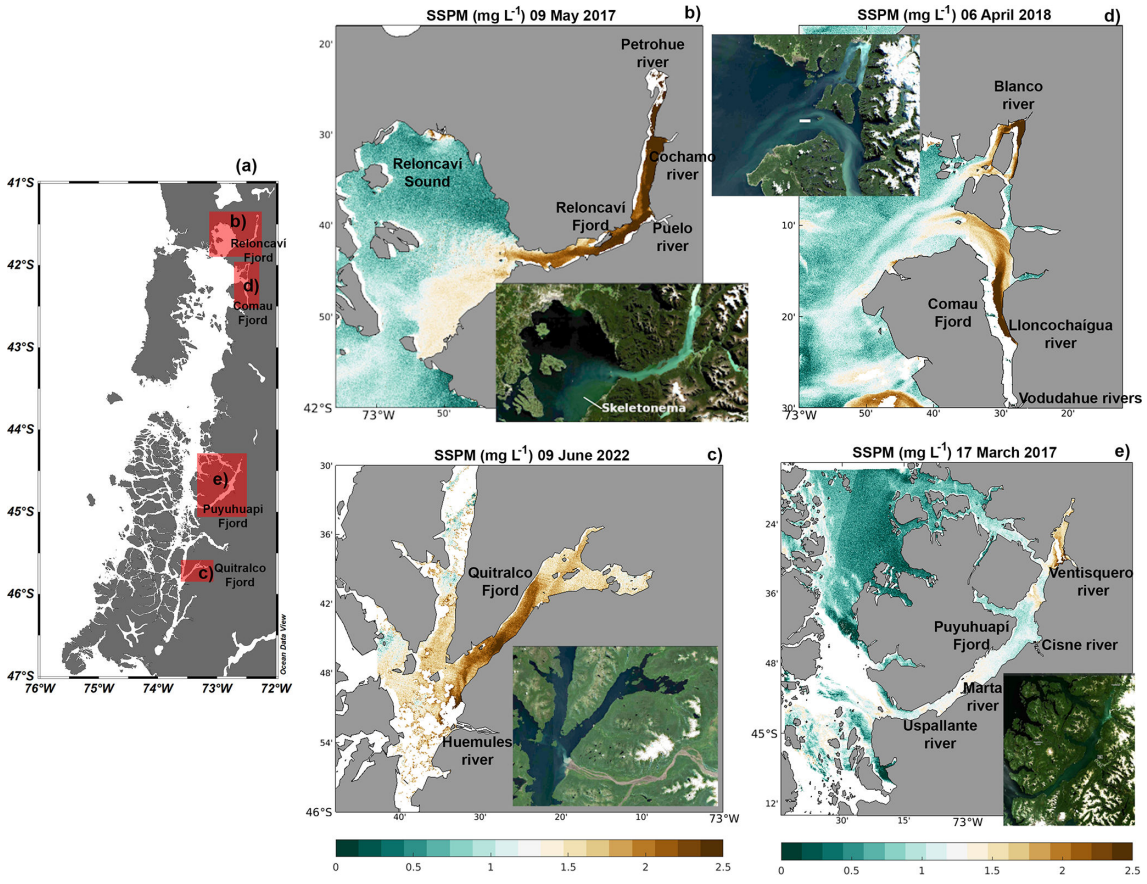



**Figure 10.** **(a)** Map showing the study sites. Satellite suspended particulate matter as measured by Sentinel-2 in **(b)** Reloncaví Sound, **(c)** the Quitralco Fjord, **(d)** the Comau Fjord, and **(e)** the Puyuhuapi Fjord. **(a)** Figure credit goes to Reiner Schlitzer, Ocean Data View, https://odv.awi.de/ (last access: September 2023) (2023).

elevation of the C : N ratio in sinking particles (Tomas et al., 1999; Schneider et al., 2003).

The spatial gradients of $\delta^{13}C$ have been previously documented in estuarine and continental shelf waters in Patagonian fjords (Silva and Vargas, 2014; Gonzalez et al., 2010; Iriarte, 2018). The horizontal–vertical distribution of the isotopic signal of $\delta^{13}C$ and $\delta^{15}N$ showed substantial variability in the northern Patagonian fjords and is the first report of data of the $\delta^{15}N$. The pronounced phytoplankton bloom (Fig. 7b) resulted in an enrichment of $\delta^{13}C$ in the upper 50 m of SPM (Fig. 11e), which is similar to observations made in other fjords around the world (Remeikaitė-Nikienė et al., 2017). The isotopic carbon signals revealed an increase in $\delta^{13}C$ values where $\%\,POC_{allo}$ decreased, indicating a shift towards a more depleted isotopic signature. This suggests the predominance of marine-derived organic carbon in areas with lower inputs of allochthonous material (Kumar et al., 2016). Moreover, the lighter carbon isotopic signals observed with depth suggest isotopic fractionation processes associated with remineralization and the preferential utilization of more labile organic carbon by heterotrophic bacteria (Muñoz et al., 2014; Kuliński et al., 2014).

The seasonal distribution of chl *a* evidenced the phytoplankton activity along the northern Patagonian fjords, especially during spring 2020 (Fig. 7). However, in the winter of 2021, a phytoplankton bloom was registered in the Reloncaví Fjord and Ancud Gulf. Pérez-Santos et al. (2021) reported the occurrence of high chl *a* and an increase in phytoplankton in Reloncaví Sound during middle and late winters (August and September 2017–2020) due to changes in the water column conditions; e.g., stratification started when salinity decreased owing to the increase in river discharge mainly caused by an early start of the ice melting. The stabilization of the water column is one of the main factors triggering primary production in the Patagonian fjords (Pérez-Santos et al., 2021).

Elevated levels of nitrogen enrichment were primarily observed in the surface layer of the region extending from the southern Chiloé inner sea to the Aysén Fjord, indicating the influence of nitrogen inputs from sources such as river discharge, atmospheric deposition, and biological activity (Velinsky and Fogel, 1999). The significant increase in nitrogen values, particularly in the Chiloé inner sea, suggests the presence of enhanced nitrogen cycling and retention

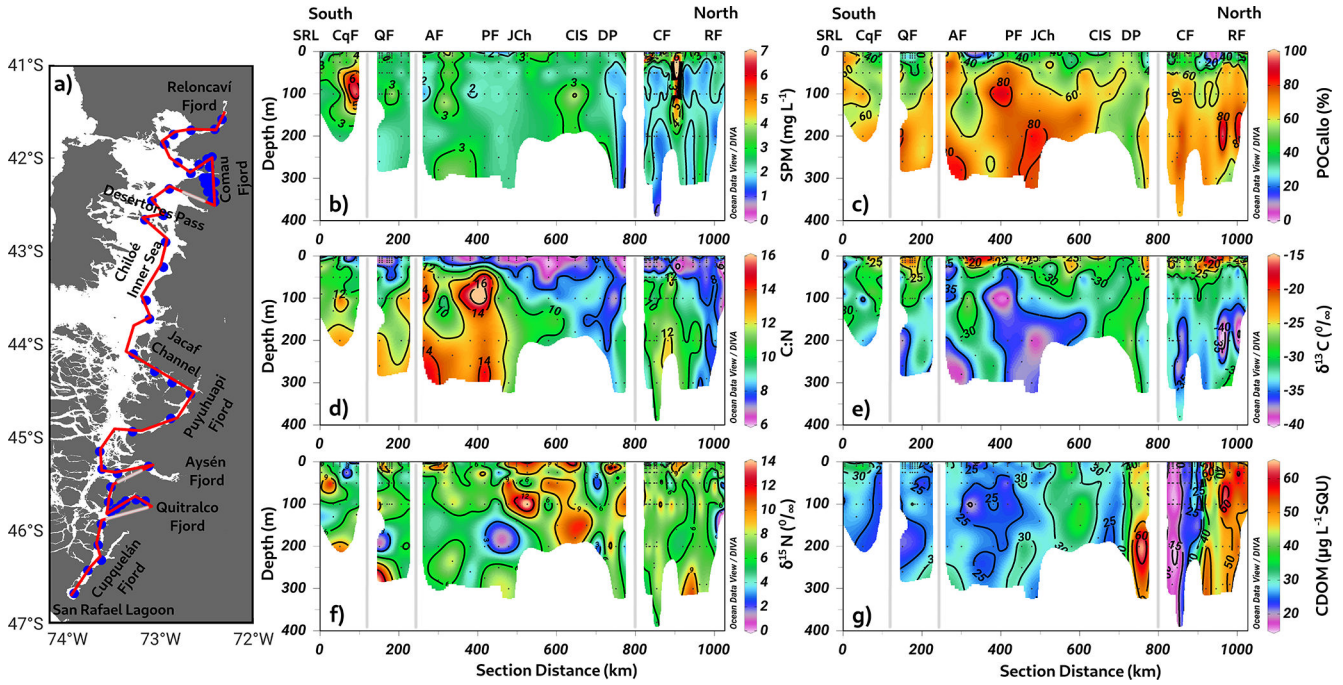



**Figure 11.** **(a)** Study area showing transects used to study biogeochemistry in November 2020 during Expedition PN-I (IFOP). **(b)** Suspended particulate material (SPM); **(c)** allochthonous carbon percentage ($POC_{allo}$); **(d)** carbon-to-nitrogen ratio (C : N); isotopic signal of **(e)** $\delta^{13}C$ and **(f)** $\delta^{15}N$; **(g)** chromophoric dissolved organic matter (CDOM). Figure credit goes to Reiner Schlitzer, Ocean Data View, https://odv.awi.de/ (last access: September 2023) (2023).

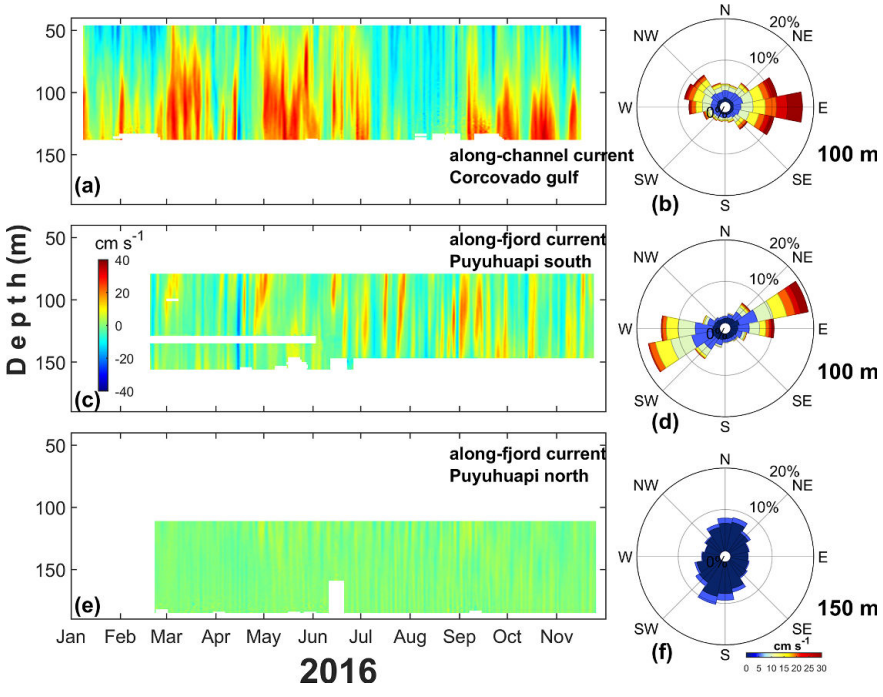



**Figure 12.** Subtidal deep circulation regimen obtained with ADCP performed in the **(a)** Gulf of Corcovado and **(c, e)** southern–northern zone of the Puyuhuapi Fjord from January to November 2016. **(b, d, f)** Marine current roses obtained at 100 m (Gulf of Corcovado), 100 m (Puyuhuapi South), and 150 m (Puyuhuapi North) depths. The location of moorings is shown in Fig. 1. In **(a)** and **(c)** the red–blue color represents the eastward–westward currents, and in **(e)** the yellow and green color represents northward–southward currents.

processes within this fjord system. This increase could result from the degradation of organic nitrogen with depth, where isotopically light $\delta^{15}$N is preferentially released from the organic matrix, leaving behind isotopically heavier residual $\delta^{15}$N (Saino and Hattori, 1980, 1987; Altabet, 1988). Similarly, the enrichment of $\delta^{15}$N in SPM suggests that primary production mainly originates from autochthonous sources in some regions of the fjords (Fig. 11). The horizontal–vertical distribution of the isotopic signal of $\delta^{13}$C and $\delta^{15}$N showed substantial variability in the northern Patagonian fjords. Our results strongly suggest that this variability was driven by biological processes, as was demonstrated by Savoye et al. (2003). They found that the co-variation in $\delta^{13}$C and $\delta^{15}$N reflects the seasonal succession of phytoplankton species due to seasonal changes in abiotic factors, such as temperature and nutrient concentration.

The distribution of CDOM in the Patagonian fjords reveals distinctive patterns, as depicted in Fig. 11. Notably, elevated CDOM concentrations were observed in the northern region, likely stemming from increased terrestrial inputs, heightened microbial activity, and prolonged CDOM residence times (Fig. 13). This phenomenon aligns with observations in fjords within the Northern Hemisphere (Mannino et al., 2008). Conversely, the southern region displays lower CDOM concentrations, indicative of diminished dissolved terrestrial inputs and potentially more efficient removal processes. It is proposed that localized CDOM concentration peaks within specific fjords signify the influence of local processes, including freshwater inputs, glacier melting, or biological production (Mannino et al., 2008), contributing significantly to the spatial heterogeneity of CDOM distribution in Patagonian fjords.

### 4.2 Mechanisms driving hypoxia and LDOW in northern Patagonian fjords

As discussed in the previous section, one of the principal mechanisms involved in the origin of hypoxic conditions in some areas of the northern Patagonian fjords was attributed to the advection of the ESSW from the Pacific Ocean to Patagonia. Recently, Linford et al. (2023) demonstrated the poleward advection of water with lower DO values by the ESSW that was transported by the Peru–Chile Undercurrent (PCUC). The passage of this water mass into the northern Patagonian fjord system was detected in a DO time series from a mooring system installed at the Guafo mouth. Moreover, as shown in Fig. 2, extreme hypoxic conditions were registered in the Quitralco Fjord, where the ESSW was absent (Fig. 6d–f).

In the Quitralco Fjord, the DO concentration was mainly governed by the biological processes of oxygen production and consumption during photosynthesis and respiration, respectively. The primary-production experiments conducted in this fjord (Figs. 8 and 9) showed higher values of community respiration than the primary production of DO (Ta-

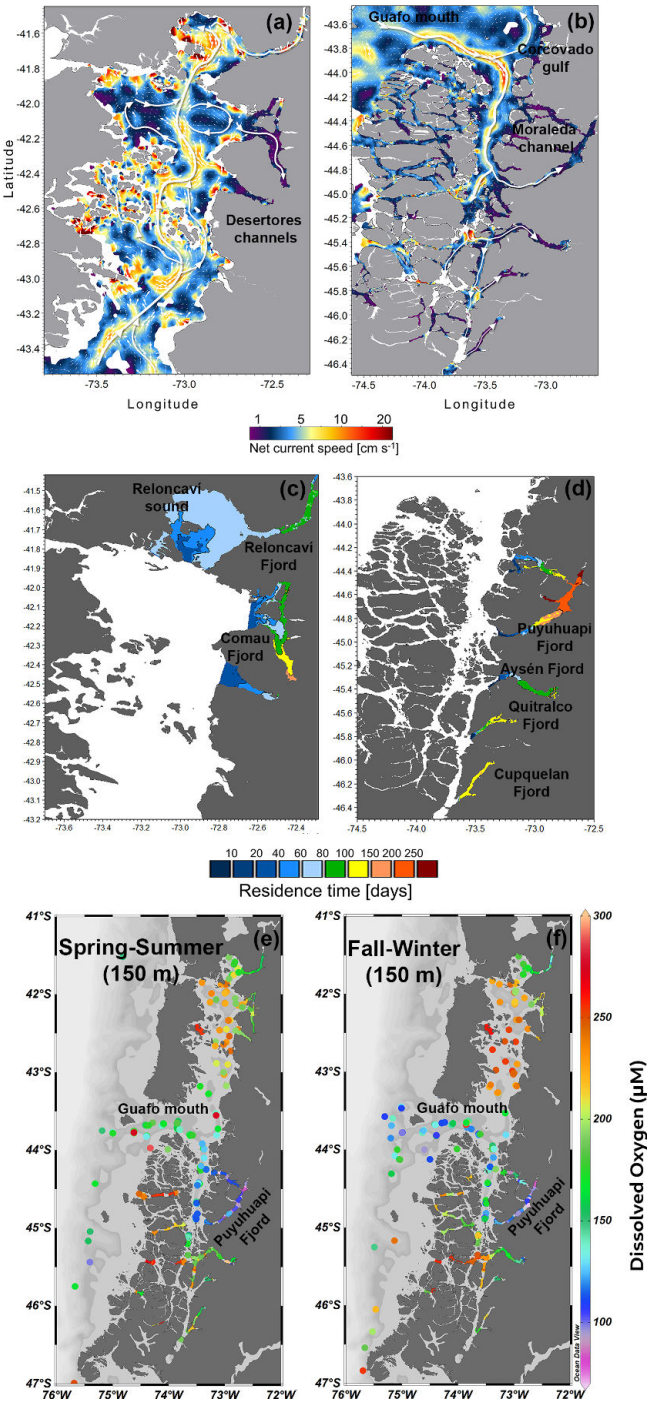



**Figure 13.** **(a, b)** Map showing the deep-current regime in the northern Patagonian fjords. The deep current was defined as subtidal currents calculated as the average of currents from 50–300 m depth. **(c, d)** The residence time calculated for each northern Patagonian fjord. **(a–d)** Data were obtained from the hydrodynamic model MIKE 3 Wave FM developed by IFOP. **(e, f)** Horizontal distribution of dissolved oxygen at a level of 150 m during spring–summer and fall–winter. Data and bathymetry are plotted in colored dots and gray. **(e, f)** Figure credit goes to Reiner Schlitzer, Ocean Data View https://odv.awi.de/ (last access: September 2023) (2023).

ble 2). In addition, the oceanographic model showed a less intense deep net current, allowing a residence time of water between 100–150 d (Fig. 13). Furthermore, satellite images provide evidence of a high concentration of suspended sediments along the Quitralco Fjord due to river discharge (Fig. 10). Regarding Magdalena Sound, the shallower hypoxia observed there (70 m depth) could be explained by the occurrence of the local upwelling produced when westerly winds blow across the mountains, as reported for the Comau Fjord by Crosswell et al. (2022) and Díaz et al. (2023) and for a temperate Canadian fjord (Jackson et al., 2023). Shallower hypoxia (10–20 m) was also registered in Clayoquot Sound, British Columbia, and was mainly attributed to local processes, such as DO consumption during the organic matter degradation, enhanced by upwelling conditions (Rosen et al., 2022).

DO concentrations in the water column are modulated by biological processes via photosynthesis (i.e., through oxygen production) and respiration/remineralization (e.g., oxygen consumption), as well as by the physiochemical properties of water (Zhang et al., 2010). In general, the production of oxygen occurs through photosynthesis in the surface waters (euphotic zone) and oxygen consumption occurs through respiration and remineralization in the entire water column. Consequently, surface waters usually contain high concentrations of oxygen as a result of photosynthesis and atmospheric exchange, whereas concentration decreases in deeper waters (Pitcher et al., 2021). In coastal waters or fjord ecosystems, owing to the high amount of organic matter (autochthonous and allochthonous) available in the water column, a greater amount of oxygen is consumed (Jackson et al., 2022) during microbial respiration (Robinson, 2019); thus heterotrophic processes dominate over autotrophic processes. Nevertheless, seasonal and spatial differences can also be observed in the dominance of these processes. This study recorded high CR rates (greater than GPP), indicating heterotrophic metabolism, where more oxygen was consumed than produced (Fig. 8). Nevertheless, the Puyuhuapi Fjord and Compu Estuary showed high oxygen production values ($GPP > 20\,mmol\,O_2\,m^{-3}\,d^{-1}$) within the 2 to 4 m layer in at least one of the two sampling periods (Fig. 8), suggesting a greater uptake than release of $CO_2$ due to the high surface primary production rates during the spring–summer period in the surface waters of some Patagonian fjords (Torres et al., 2011). A recent global assessment of $CO_2$ uptake from estuaries, including tidal systems and deltas, lagoons, and fjords, reported that fjord ecosystems can reduce 37 % of $CO_2$ anthropogenic emissions (Rosentreter et al., 2023). DO and organic matter are produced only in the well-lit upper ocean but can be consumed throughout the water column. Therefore, in areas of high surface production and slow resupply of oxygen at depth (compared to the rate at which oxygen is respired), DO concentrations may be reduced to hypoxic levels at depth. Nevertheless, sporadic deep-water renewal was observed close to the bottom (160–180 m) in the Puyuhuapi Fjord owing to the inflow of dense water above the sill favoring the ventilation and inhibiting the occurrence of deep anoxia conditions (Pinilla et al., 2020), as also reported by Jackson et al. (2022) in Rivers Inlet, British Columbia, and on the west coast of Vancouver Island (Thomson et al., 2017). The first map of residence time in the northern Patagonian fjord shows a coincidence of the area where a high residence time was reported (100–250 d) with the depleted oxygen region, for example, hypoxic and LDOW areas (Fig. 13). The hydrodynamic model and derived calculations are helpful tools for explaining the oxygen distribution and patterns in the northern Patagonian fjord system.

## 5 Conclusions

Since the beginning of oceanographic research in the Patagonian fjords (1970), hypoxia and LDOW have been reported along the water column. A dataset of hydrographic–biogeochemical parameters, in situ experiments of primary production/community respiration, satellite suspended particulate matter, and the output of a hydrodynamic model allowed for a holistic evaluation of the oceanographic and biogeochemical processes contributing to hypoxia and LDOW in Patagonian subsurface waters. The influence of the ESSW was recognized as one of the first drivers of this phenomenon. This water mass transported poleward poorly oxygenated waters that entered the northern Patagonian fjords through the Guafo mouth and moved southward through the Moraleda and Jacaf channels and the Puyuhuapi Fjord. The distribution of the ESSW inside the northern Patagonian fjords coincides with the most extensive zone of the LDOW records. However, the hypoxic conditions registered in this zone were also attributed to the high rate of DO consumption during community respiration processes, owing to the entrance of allochthonous organic matter (natural and/or anthropogenic) to the fjords. Additionally, the results from marine currents derived from ADCP measurements and the hydrodynamic model demonstrated a weak water circulation and a long residence time that led to slow deep-water ventilation, resulting in a drop in the DO level and, finally, the occurrence of hypoxic conditions. The Quitralco Fjord also reported hypoxic conditions showing the absolute minimum of DO with $9.36\,\mu mol\,L^{-1}$ and 1.6 % oxygen saturation. The ESSW was not observed in this area. Therefore, the presence of hypoxic water in the deep layer of Quitralco was attributed to weak deep-water circulation and a long residence time, together with a high rate of DO consumption by community respiration and a higher supply of allochthonous organic matter due to river discharge. Similar processes favoring LDOW were registered at the Aysén, Comau, and Reloncaví fjords, but in the Reloncaví systems, marine currents and residence times were significantly higher than in other fjords. The presence of LDOW in the Reloncaví systems responded mainly to biological processes, e.g., DO consumption during com-

munity respiration by phytoplankton and remineralization by bacteria. The analyses of the processes contributing to hypoxic conditions and LDOW in the water column of northern Patagonian fjords allowed for the identification of the main causes leading to oxygen loss in each fjord investigated. The results provide the environmental information needed to contribute to the sustainable management of the northern Patagonian fjord considering anthropogenic activities and climate change scenarios. In addition, they provide significant information for understanding the life cycle of marine species that inhabit Patagonian fjords. Finally, our study provides valuable insights into the relationship between hypoxia, low-oxygen processes, the origin of organic carbon, isotopic signals of carbon and nitrogen, the C : N ratio, and the presence of CDOM in the Patagonian fjords. These findings highlight the complex interactions between terrestrial and marine processes and emphasize the role of fjords as potential sites for hypoxia and the accumulation of organic matter. Understanding these relationships is crucial for accurately assessing the impact of low-oxygen processes and carbon cycle dynamics in fjord ecosystems and their contribution to the global carbon cycle. Further research is needed to elucidate the mechanisms driving these patterns and their implications for the functioning of fjord ecosystems and their resilience to continuous environmental changes.

*Data availability.* All datasets used in this paper can be requested from the corresponding author.

*Supplement.* The supplement related to this article is available online at: https://doi.org/10.5194/bg-21-1433-2024-supplement.

*Author contributions.* PL: study design, data analysis, and manuscript leader. IPS: study design, collection, analysis of physical oceanographic data, and manuscript leader. PM: study design, collection, and analysis of primary-production data. PD: study design, collection, and analysis of physical–biological oceanographic data. CA: collection and analysis of primary-production data. EP: development of oceanographic model and analysis of physical oceanographic data. FB: collection and analysis of biogeochemical data. MC: analysis of marine current data. AA: study design, collection, and analysis of satellite data. MA: collection and analysis of marine current data. GS: study design, collection, and analysis of physical oceanographic data. CP: edition and analysis of satellite data. CS: collection and analysis of physical oceanographic data. SA: collection and analysis of biogeochemical data. PN: collection, and analysis of biogeochemical data. GM: collection of physical, biological, and biogeochemical data. RA: collection of physical, biological, and biogeochemical data. JSM: processing and analysis of model data for residence time. CSR: validation of hydrodynamic model. All authors contributed to the writing of the manuscript.

*Competing interests.* The contact author has declared that none of the authors has any competing interests.

*Disclaimer.* Publisher's note: Copernicus Publications remains neutral with regard to jurisdictional claims made in the text, published maps, institutional affiliations, or any other geographical representation in this paper. While Copernicus Publications makes every effort to include appropriate place names, the final responsibility lies with the authors.

*Special issue statement.* This article is part of the special issue "Low-oxygen environments and deoxygenation in open and coastal marine waters". It is a result of the 53rd International Colloquium on Ocean Dynamics (3rd GO2NE Oxygen Conference), Liège, Belgium, 16–20 May 2022.

*Acknowledgements.* We thank the CHONOS initiative of the Instituto de Fomento Pesquero (IFOP) for facilitating the use of its computer systems to access the MIKE 3, WRF, and FLOW models and the Ministry of Economy, Development and Tourism of the Chilean government for funding through the Undersecretariat for Fisheries and Aquaculture. Elias Pinilla would like to acknowledge funding from the National Science Foundation (NSF grant number 2045866). We acknowledge Ocean Data View software (Reiner Schlitzer, Ocean Data View, https://odv.awi.de/ (last access: September 2023), 2023) for the data analysis and the construction of figures in the paper.

*Financial support.* This research was funded by FONDECYT 1211037 and partially funded by COPAS Sur-Austral ANID AFB170006, the Office of Naval Research grant N00014-17-1-2606, COPAS COASTAL FB210021, and CIEP R20F002. Facundo Barrera was funded by FONDECYT 31308. Cécile Pujol was financially supported by the F.R.S.-FNRS (Fonds de la Recherche Scientifique de Belgique, Communauté Française de Belgique) through a FRIA grant. Patricio A. Díaz was funded by the Centre for Biotechnology and Bioengineering (CeBiB) (PIA project FB0001, ANID, Chile). Manuel Castillo was funded by CS2018-7929 and ATE220033.

*Review statement.* This paper was edited by Lisa Levin and reviewed by Jennifer Jackson and one anonymous referee.

## References

Aiken, C. M.: Seasonal thermal structure and exchange in Baker Channel, Chile, Dynam. Atmos. Ocean., 58, 1–19, https://doi.org/10.1016/j.dynatmoce.2012.07.001, 2012.

Andrejev, O., Myrberg, K., and Lundberg, P. A.: Age and renewal time of water masses in a semi-enclosed basin – application to the Gulf of Finland, Tellus A, 56, 548–558, https://doi.org/10.3402/tellusa.v56i5.14435, 2004.

Altabet, M. A.: Variations in nitrogen isotopic composition between sinking and suspended particles: implication for nitrogen cycling and particle transformation in the open ocean, Deep-Sea Res., 35, 535–554, 1988.

Andrewartha, H. G. and Birch, L. C.: The ecological web: more on the distribution and abundance of animals, University of Chicago Press, ISBN 0226020347, 9780226020341, 1986.

Barrera, F., Lara, R., and Krock, J.: Factors influencing characteristics and distribution of organic particles and macromolecules in the Pacific-Atlantic connection, J. Mar. Syst., 175, 36–45, https://doi.org/10.1016/j.jmarsys.2017.07.004, 2017.

Batiuk, R. A., Breitburg, D. L., Diaz, R. J., Cronin, T. M., Secor, D. H., and Thursby, G.: Derivation of habitat-specific dissolved oxygen criteria for Chesapeake Bay and its tidal tributaries, J. Exp. Mar. Biol. Ecol., 381, 204–215, https://doi.org/10.1016/j.jembe.2009.07.023, 2009.

Bianchi, T. S.: Biogeochemistry of estuaries. Oxford University Press on Demand, ISBN 0196160827, 9780195160826, 2007.

Bianchi, T. S., DiMarco, S. F., Cowan, J. H., Hetland, R. D., Chapman, P. D., and Allison, J. W.: The science of hypoxia in the Northern Gulf of Mexico: A review, Sci. Total Environ., 408, 1471–1484, https://doi.org/10.1016/j.scitotenv.2009.11.047, 2010.

Billi, M., Mascareño, A., Henríquez, P. A., Rodríguez, I., Padilla, F., and Ruz, G. A.: Learning from crises?, The long and winding road of the salmon industry in Chiloé Island, Chile, Mar. Policy, 140, 105069, https://doi.org/10.1016/j.marpol.2022.105069, 2022.

Breitburg, D. L., Loher, T., Pacey, C. A., and Gerstein, A.: Varying effects of low dissolved oxygen on trophic interactions in an estuarine food web, Ecol. Monogr., 67, 489–507, https://doi.org/10.1890/0012-9615(1997)067[0489:VEOLDO]2.0.CO;2, 1997.

Breitburg, D., Levin, L. A., Oschlies, A., Grégoire, M., Chavez, F. P., Conley, D. J., and Zhang, J.: Declining oxygen in the global ocean and coastal waters, Science, 359, 6371, https://doi.org/10.1126/science.aam7240, 2018.

Castillo, M. I., Cifuentes, U., Pizarro, O., Djurfeldt, L., and Caceres, M.: Seasonal hydrography and surface outflow in a fjord with a deep sill: the Reloncaví fjord, Chile, Ocean Sci., 12, 533–544, https://doi.org/10.5194/os-12-533-2016, 2016.

Carrasco, C. and Silva, N.: Comparación de las características oceanográficas físicas y químicas presente en la zona de Puerto Montt a la boca del Guafo entre el invierno y la primavera de 2004 y entre las primaveras de 1995 y 2004, Cienc. Tecnol. del Mar, 33, 17–44, 2010.

Conley, D. J., Paerl, H. W., Howarth, R. W., Boesch, D. F., Seitzinger, S. P., Havens, K. E., and Likens, G. E.: Controlling eutrophication: nitrogen and phosphorus, Science, 323, 1014–1015, https://doi.org/10.1126/science.1167755, 2009.

Crosswell, J. R., Bravo, F., Pérez-Santos, I., Carlin, G., Cherukuru, N., Schwarger, C., Gregor, R., and Steven, A.: Geophysical controls on metabolic cycling in three Patagonian fjords, Prog. Oceanogr., 207, 102866, https://doi.org/10.1016/j.pocean.2022.102866, 2022.

Davis, J. C.: Minimal dissolved oxygen requirements of aquatic life with emphasis on Canadian species: a review, J. Fish. Board Can., 32, 2295–2332, https://doi.org/10.1139/f75-268, 1975.

Díaz, R. J.: Overview of hypoxia around the world, J. Environ. Qual., 30, 275–281, https://doi.org/10.2134/jeq2001.302275x, 2001.

Diaz, R. J. and Rosenberg, R.: Marine benthic hypoxia: a review of its ecological effects and the behavioural responses of benthic macrofauna, Oceanography and marine biology, Annu. Rev., 33, 245, 1995.

Díaz, P., Pérez-Santos, I., Álvarez, G., Garreaud, R., Pinilla, E., Díaz, M., Sandoval, A., Araya, M., Álvarez, F., Rengel, J., Montero, P., Pizarro, G., López, L., Iriarte, L., Igor, G., and Reguera, B.: Multiscale physical background to an exceptional harmful algal bloom of Dinophysis acuta in a fjord system, Sci. Total Environ., 773, 145621, https://doi.org/10.1016/j.scitotenv.2021.145621, 2021.

Díaz, P. A., Pérez-Santos, I., Basti, L., Garreaud, R., Pinilla, E., Barrera, F., and Figueroa, R. I.: The impact of local and climate change drivers on the formation, dynamics, and potential recurrence of a massive fish-killing microalgal bloom in Patagonian fjord, Sci. Total Environ., 865, 161288, https://doi.org/10.1016/j.scitotenv.2022.161288, 2023.

Ekau, W., Auel, H., Pörtner, H.-O., and Gilbert, D.: Impacts of hypoxia on the structure and processes in pelagic communities (zooplankton, macro-invertebrates and fish), Biogeosciences, 7, 1669–1699, https://doi.org/10.5194/bg-7-1669-2010, 2010.

Fuenzalida, R., Schneider, W., Garcés-Vargas, J., Bravo, L., and Lange, C.: Vertical and horizontal extension of the oxygen minimum zone in the eastern South Pacific Ocean, Deep-Sea Res. Pt. II, 56, 992–1003, https://doi.org/10.1016/j.dsr2.2008.11.001, 2009.

Fry, B. and Sherr, E. B.: $\delta^{13}$C measurements as indicators of carbon flow in marine and freshwater ecosystems, Ecol. Stud., 68, 196–229, https://doi.org/10.1007/978-1-4612-3498-2_12, 1989.

González, H. E., Calderón, M. J., Castro, L., Clement, A., Cuevas, L. A., Daneri, G., and Molinet, C.: Primary production and plankton dynamics in the Reloncaví Fjord and the Interior Sea of Chiloé, Northern Patagonia, Chile, Mar. Ecol. Prog. Ser., 402, 13–30, https://doi.org/10.3354/meps08360, 2010.

González, H. E., Nimptsch, J., Giesecke, R., and Silva, N.: Organic matter distribution, composition and its possible fate in the Chilean North-Patagonian estuarine system, Sci. Total Environ., 657, 1419–1431, https://doi.org/10.1016/j.scitotenv.2018.11.445, 2019.

Grasshoff, K., Ehrhardt, M., and Kremling, K.: Methods of Seawater Analysis, (2nd edition), Verlag Chemie Weinhein, New York, USA, ISBN 3-527-29589-5, 1983.

Grasshoff, K., Kremling, K., and Ehrhardt, M. (Eds.): Methods of seawater analysis, John Wiley and Sons, ISBN 3527613994, 9783527613991, 2009.

Harmelin-Vivien, M., Loizeau, V., Mellon, C., Beker, B., Arlhac, D., Bodiguel, X., Ferraton, T., Hermand, R., Philippon, X., and Salen-Picard, C.: Comparison of C and N stable isotope ratios between surface particulate organic matter and microphytoplankton in the Gulf of lions (NW Mediterranean), Cont. Shelf Res., 28, 1911–1919, https://doi.org/10.1016/j.csr.2008.03.002, 2008.

Holding, J. M., Duarte, C. M., Delgado-Huertas, A., Soetaert, K., Vonk, J. E., Agustí, S., Wassmann, P., and Middelburg, J. J.: Autochthonous and allochthonous contributions of organic carbon to microbial food webs in Svalbard fjords, Limnol. Oceanogr., 62, 1307–1323, https://doi.org/10.1002/lno.10526, 2017.

Guzmán, D. and Silva, N.: Caracterización física y química y masas de agua en los canales australes de Chile entre boca del Guafo y estero Elefantes (crucero CIMAR 4 Fiordos), Cienc. Tecnol. Mar., 25, 45–76, 2002.

IOC, S.: IAPSO: The international thermodynamic equation of seawater–2010: Calculation and use of thermodynamic properties, Intergovernmental Oceanographic Commission, Manuals and Guides No. 56, UNESCO, Manuals and Guides, 56, 1–196, 2010.

Iriarte, J. L.: Natural and human influences on marine processes in Patagonian Subantarctic coastal waters, Front. Mar. Sci., 5, 360, https://doi.org/10.3389/fmars.2018.00360, 2018.

Iriarte, J. L., Gonzalez, H. E., Liu, K. K., Rivas, C., and Valenzuela, C. P.: Spatial and temporal variability of chlorophyll and primary productivity in surface waters of southern Chile, Estuar. Coast. Shelf Sci., 74, 471e480, https://doi.org/10.1016/j.ecss.2007.05.015, 2017.

Jackson, J. M. Johannessen, S., Belluz, J., Hunt, B., and Hannah, C.: Identification of a Seasonal Subsurface Oxygen Minimum in Rivers Inlet, British Columbia, Estuar. Coast., 45, 754–771, https://doi.org/10.1007/s12237-021-00999-y, 2022.

Jackson, J. M., Holmes, K., Klymak, J. M., Bianucci, L., Evans, W., Floyd, W. C., Hannah, C., Hare, A., and Wan, D.: Winter Arctic outflow winds cause upper ocean cooling and reoxygenation in a temperate Canadian fjord, Geophys. Res. Lett., 50, e2023GL104549, https://doi.org/10.1029/2023GL104549, 2023.

Kattner, G. and Becker, H.: Nutrients and organic nitrogenous compounds in the marginal ice zone of the Fram Strait, J. Mar. Syst., 2, 385–394, https://doi.org/10.1016/0924-7963(91)90043-T, 1991.

Kumar, V., Tiwari, M., Nagoji, S., Tripathi, S.Kumar, V., Tiwari, M., Nagoji, S. et al. Evidence of Anomalously Low $\delta^{13}$C of Marine Organic Matter in an Arctic Fjord, Sci. Rep., 6, 36192, https://doi.org/10.1038/srep36192, 2016.

Kuliński, K., Kędra, M., Legeżyńska, J., Gluchowska, M., and Zaborska, A.: Particulate organic matter sinks and sources in high Arctic fjord, J. Mar. Syst., 139, 27–37, https://doi.org/10.1016/j.jmarsys.2014.04.018, 2014.

Kutty, M. N.: Respiratory quotients in goldfish and rainbow trout, J. Fish. Board Can., 25, 1689–1728, https://doi.org/10.1139/f68-150, 1968.

Laffoley, D. and Baxter, J. M.: Ocean deoxygenation: Everyone's problem-Causes, impacts, consequences and solutions, Gland, Switzerland, IUCN, https://doi.org/10.2305/IUCN.CH.2019.13.en, 2019.

Landaeta, M. F., Gómez, A., Contreras, J. E., Figueroa-González, Y., Pinilla, E., Reche, P., Castillo, M. I., and Plaza, G.: Linking shape and growth in young-of-the-year rock fish: an ecological carry-over effect?, Mar. Biol., 170, 103, https://doi.org/10.1007/s00227-023-04248-7, 2023.

Lefort, S.: A multidisciplinary study of hypoxia in the deep water of the Estuary and Gulf of St. Lawrence: Is this ecosystem on borrowed time?, McGill University (Canada), PhD Thesis Department of Earth and Planetary Sciences McGill University, Montreal, 2012.

Linford, P., Pérez-Santos, I., Montes, I., Dewitte, B., Buchan, S., Narváez, D., Saldías, G., Pinilla, E., Garreaud, R., Díaz, P., Schwertes, C., Montero, P., Rodríguez-Villegas, C., Cáceres-Soto M., Mancilla-Gutiérrez, G., and Altamirano, R.: Recent deoxygenation of Patagonian fjord subsurface waters connected to the Peru–Chile undercurrent and equatorial subsurface water variability, Global Biogeochem. Cy., 37, e2022GB007688, https://doi.org/10.1029/2022GB007688, 2023.

Mannino, A., Russ, M. E., and Hooker, S. B.: Algorithm development and validation for satellite-derived distributions of DOC and CDOM in the U.S. Middle Atlantic Bight, J. Geophys. Res., 113, C07051, https://doi.org/10.1029/2007JC004493, 2008.

Mardones, J. I., Paredes, J., Godoy, M., Suarez, R., Norambuena, L., Vargas, V., Fuenzalida, G., Pinilla, E., Artal, O., Rojas, X., Dorantes-Aranda, J. J., Lee Chang, K. J., Anderson, D. M., and Hallegraeff, G. M.: Disentangling the environmental processes responsible for the world's largest farmed fish-killing harmful algal bloom: Chile, 2016, Sci. Total Environ., 766, 144383, https://doi.org/10.1016/j, 2021.

Martínez, D., De Lázaro, O., Cortés, P., Oyarzún-Salazar, R., Paschke, K., and Vargas-Chacoff, L.: Hypoxia modulates the transcriptional immunological response in Oncorhynchus kisutch, Fish Shellf. Immun., 106, 1042–1051, https://doi.org/10.1016/j.fsi.2020.09.025, 2020.

Meire, L., Soetaert, K. E. R., and Meysman, F. J. R.: Impact of global change on coastal oxygen dynamics and risk of hypoxia, Biogeosciences, 10, 2633–2653, https://doi.org/10.5194/bg-10-2633-2013, 2013.

Monsen, N. E., Cloern, J. E., Lucas, L. V., and Monismith, S. G.: A comment on the use of flushing time, residence time, and age as transport time scales, Limnol. Oceanogr., 47, 1545–1553, https://doi.org/10.4319/lo.2002.47.5.1545, 2002.

Montero, P., Daneri, G., Gonzalez, H. E., Iriarte, J. L., Tapia, F. J., Lizarraga, L., and Pizarro, O.: Seasonal variability of primary production in a fjord ecosystem of the Chilean Patagonia: Implications for the transfer of carbon within pelagic food webs, Cont. Shelf Res., 31, 202–215, https://doi.org/10.1016/j.csr.2010.09.003, 2011.

Montero, P., Pérez-Santos, I., Daneri, G., Gutiérrez, M. H., Igor, G., Seguel, R., and Crawford, D. W.: A winter dinoflagellate bloom drives high rates of primary production in a Patagonian fjord ecosystem, Estuarine, Coast. Shelf Sci., 199, 105–116, https://doi.org/10.3856/vol45-issue5-fulltext-16, 2017a.

Montero, P., Daneri, G., Tapia, F., Iriarte, J. L., and Crawford, D.: Diatom blooms and primary production in a channel ecosystem of central Patagonia, Lat. Am. J. Aquat. Res., 45, 999–1016, https://doi.org/10.3856/vol45-issue5-fulltext-16, 2017b.

Montero, P., Gutiérrez, M. H., Daneri, G., and Jacob, B.: The Effect of Salmon Food-Derived DOM and Glacial Melting on Activity and Diversity of Free-Living Bacterioplankton in Chilean Patagonian Fjords, Front. Microbiol., 12, 772900, https://doi.org/10.3389/fmicb.2021.772900, 2022.

Nechad, B., Dogliotti, A., Ruddick, K., and Doxaran, D.: Particulate backscattering and suspended matter concentration retrieval from remote-sensed turbidity in various coastal and riverine turbidy waters, Submitted for the Proceedings of ESA Living Planet Symposium, Prague, 9–13 May 2016, ESA-SP 740, 2016.

Nimptsch, J., Woelfl, S., Osorio, S., Valenzuela, J., Ebersbach, P., von Tuempling, W., and Graeber, D.: Tracing dissolved organic matter (DOM) from land-based aquaculture systems in North Patagonian streams, Sci. Total Environ., 537, 129–138, https://doi.org/10.1016/j.scitotenv.2015.07.160, 2015.

Oschlies, A., Brandt, P., Stramma, L., and Schmidtko, S.: Drivers and mechanisms of ocean deoxygenation, Nat. Geosci., 11, 467–473, https://doi.org/10.1038/s41561-018-0152-1, 2018.

Paulmier, A. and Ruiz-Pino, D.: Oxygen minimum zones (OMZs) in the modern ocean, Prog. Oceanogr., 80, 113–128, https://doi.org/10.1016/j.pocean.2008.08.001, 2009.

Pawlowicz, R., Beardsley, B., and Lentz, S.: Classical tidal harmonic analysis including error estimates in MATLAB using T_TIDE, Comput. Geosci., 28, 929–937, https://doi.org/10.1016/S0098-3004(02)00013-4, 2002.

Pérez-Santos, I., Garcés-Vargas, J., Schneider, W., Ross, L., Parra, S., and Valle-Levinson, A.: Double-diffusive layering and mixing in Patagonian fjords, Prog. Oceanogr., 129, 35–49, https://doi.org/10.1016/j.pocean.2014.03.012, 2014.

Pérez-Santos, I., Castro, L., Ross, L., Niklitschek, E., Mayorga, N., Cubillos, L., Gutierrez, M., Escalona, E., Castillo, M., Alegría, N., and Daneri, G.: Turbulence and hypoxia contribute to dense biological scattering layers in a Patagonian fjord system, Ocean Sci., 14, 1185–1206, https://doi.org/10.5194/os-14-1185-2018, 2018.

Pérez-Santos, I., Seguel, R., Schneider, W., Linford, P., Donoso, D., Navarro, E., Amaya-Cárcamo, C., Pinilla, E., and Daneri, G.: Synoptic-scale variability of surface winds and ocean response to atmospheric forcing in the eastern austral Pacific Ocean, Ocean Sci., 15, 1247–1266, https://doi.org/10.5194/os-15-1247-2019, 2019.

Pérez-Santos, I., Díaz, P., Silva, N., Garreaud, R., Montero, P., Henríquez-Castillo, C., Barrera, F., Linford, P., Amaya, C., Contreras, S., Aracena, C., Pinilla, E., Altamirano, R., Vallejos, L., Pavez, J., and Maulen, J.: Oceanography time series reveals annual asynchrony input between oceanic and estuarine waters in Patagonian fjords, Sci. Total Environ., 798, 149241, https://doi.org/10.1016/j.scitotenv.2021.149241, 2021.

Pinilla, E., Castillo, M. I., Pérez-Santos, I., Venegas, O., and Valle-Levinson, A.: Water age variability in a Patagonian fjord, J. Mar. Syst., 210, 103376, https://doi.org/10.1016/j.jmarsys.2020.103376, 2020.

Prandle, D.: Simple theory for designing tidal power schemes, Adv. Water Res., 7, 21–27, https://doi.org/10.1016/0309-1708(84)90026-5, 1984.

Quiñones, R. A., Fuentes, M., Montes, R. M., Soto, D., and León-Muñoz, J.: Environmental issues in Chilean salmon farming: a review, Rev. Aquacult., 11, 375–402, https://doi.org/10.1111/raq.12337, 2019.

Rabalais, N. N., Díaz, R. J., Levin, L. A., Turner, R. E., Gilbert, D., and Zhang, J.: Dynamics and distribution of natural and human-caused hypoxia, Biogeosciences, 7, 585–619, https://doi.org/10.5194/bg-7-585-2010, 2010.

Remeikaitė-Nikienė, N., Lujanienė, G., Malejevas, V., Barisevičiūtė, R., Zilius, M., Vybernaitė-Lubienė, I., and Stankevičius, A.: Assessing nature and dynamics of POM in transitional environment (the Curonian Lagoon, SE Baltic Sea) using a stable isotope approach, Ecol. Indicat., 82, 217–226, https://doi.org/10.1016/j.ecolind.2017.06.035, 2017.

Reche, P., Artal, O., Pinilla, E., Ruiz, C., Venegas, O., Arriagada, A., and Falvey, M.: CHONOS: oceanographic information website for Chilean Patagonia, Ocean Coast Manag., 208, 105634, https://doi.org/10.1016/j.ocecoaman.2021.105634, 2021.

Redfield, A. C.: The biological control of chemical factors in the environment, Am. Sci., 46, 230–221, 1958.

Robinson, C.: Microbial respiration, the engine of ocean deoxygenation, Front. Mar. Sci., 5, 533, https://doi.org/10.3389/fmars.2018.00533, 2019.

Rosentreter, J., Laruelle, G., Bange, H., Bianchi, T., Busecke, J., Cai, W., Eyre, B., Forbrich, I., Kwon, E., Maavara, T., Moosdorf, N., Najjar, R., Sarma, V., Van Dam, B., and Regnier, P.: Coastal vegetation and estuaries are collectively a greenhouse gas sink, Nat. Clim. Change, 13, 579–587, https://doi.org/10.1038/s41558-023-01682-9, 2023.

Rosen, S., Bianucci, L., Jackson, J. M., Hare, A., Greengrove, C., Monks, R., Bartlett, M., and Dick, J.: Seasonal near-surface hypoxia in a temperate fjord in Clayoquot Sound, British Columbia, Front. Mar. Sci., 9, 1000041, https://doi.org/10.3389/fmars.2022.1000041, 2022.

Ruiz, C., Artal, O., Pinilla, E., and Sepúlveda, H. H.: Stratification and mixing in the Chilean Inland Sea using an operational model, Ocean Modell., 158, 101750, https://doi.org/10.1016/j.ocemod.2020.101750, 2021.

Sampaio, E., Santos, C., Rosa, I. C., Ferreira, V., Pörtner, H. O., Duarte, C. M., and Rosa, R.: Impacts of hypoxic events surpass those of future ocean warming and acidification, Nat. Ecol. Evol., 5, 311–321, https://doi.org/10.1038/s41559-020-01370-3, 2021.

Saino, T. and Hattori, A.: $^{15}$N natural abundance in oceanic suspended particulate matter, Nature, 283, 752–754, 1980.

Saino, T. and Hattori, A.: Geographical variation of the water column distribution of suspended particulate nitrogen and its $^{15}$N natural abundance in the Pacific and its marginal seas, Deep-Sea Res., 34, 807–827, 1987.

Savoye, N., Aminot, A., Treguer, P., Fontugne, M., Naulet, N., and Kérouel, R.: Dynamics of particulate organic matter $\delta^{15}$N and $\delta^{13}$C during spring phytoplankton blooms in a macrotidal ecosystem (Bay of Seine, France), Mar. Ecol. Prog. Ser., 255, 27–41, 2003.

Schmidtko, S., Stramma, L., and Visbeck, M.: Decline in global oceanic oxygen content during the past five decades, Nature, 542, 335–339, https://doi.org/10.1038/nature21399, 2017.

Schneider, W., Pérez-Santos, I., Ross, L., Bravo, L., Seguel, R., and Hernández, F.: On the hydrography of Puyuhuapi Channel, Chilean Patagonia, Prog. Oceanogr., 129, 8–18, https://doi.org/10.1016/j.pocean.2014.03.007, 2014.

Schneider, B., Schlitzer, R., Fischer, G., and Nothig, E. M.: Depth-dependent elemental compositions of particulate organic matter (POM) in the ocean, Glob. Biogeochem. Cy., 17, 1032, https://doi.org/10.1029/2002gb001871, 2003.

Sibson, R. and Thomson, G. D.: A seamed quadratic element for contouring, Comput. J., 24, 378–382, https://doi.org/10.1093/comjnl/24.4.378, 1981.

Sievers, H. A.: Temperature and salinity in the austral Chilean channels and fjords, Progress in the oceanographic knowledge of Chilean interior waters, from Puerto Montt to Cape Horn, Comité Oceanográfico Nacional-Pontificia Universidad Católica de Valparaíso, Valparaíso, 31–36, 2008.

Sievers, A. H. and Silva, N.: Water masses and circulation in austral Chilean channels and fjords, in: Progress in the oceanographic knowledge of Chilean inner waters, from Puerto Montt to Cape Horn, edited by: Silva, N. and Palma, S., Comité Oceanografico Nacional, Pontificia Universidad Católica de Val-

paraíso, Valparaíso, 53–58, http://www.cona.cl/ (last access: September 2022), 2008.

Silva, N.: Physical and chemical characteristics of the surface sediments in the austral Chilean channels and fjords, Progress in the oceanographic knowledge of Chilean interior waters, from Puerto Montt to Cape Horn, 69–75, http://www.cona.mil.cl/ (last access: September 2022), 2008.

Silva, N. and Vargas, C. A.: Hypoxia in Chilean patagonian fjords, Prog. Oceanogr., 129, 62–74, https://doi.org/10.1016/j.pocean.2014.05.016, 2014.

Silva, N., Rojas, N., and Fedele, A.: Water masses in the Humboldt Current System: Properties, distribution, and the nitrate deficit as a chemical water mass tracer for Equatorial Subsurface Water off Chile, Deep-Sea Res. Pt. II, 56, 1004–1020, https://doi.org/10.1016/j.dsr2.2008.12.013, 2009.

Smith, D. C. and Azam, F.: A simple, economical method for measuring bacterial protein synthesis rates in seawater using 3H-leucine, Mar. Microb. Food Webs, 6, 107–114, 1992.

Sibson, R.: A Brief Description of Natural Neighbor Interpolation, edited by: Barnett, V., Interpreting Multivariate Data, John Wiley & Sons, New York, 21–36, 1981.

Soto, D. and Norambuena, F.: Evaluation of salmon farming effects on marine systems in the inner seas of southern Chile: a large-scale mensurative experiment, J. Appl. Ichthyol., 20, 493–501, https://doi.org/10.1111/j.1439-0426.2004.00602, 2004.

Soto, D., León-Muñoz, J., Garreaud, R., Quiñones, R. A., and Morey, F.: Scientific warnings could help to reduce farmed salmon mortality due to harmful algal blooms, Mar. Pol., 132, 104705, https://doi.org/10.1016/j.marpol.2021.104705, 2021.

Soto-Riquelme, C., Pinilla, E., and Ross, L.: Wind influence on residual circulation in Patagonian channels and fjords, Cont. Shelf Res., 254, 104905, https://doi.org/10.1016/j.csr.2022.104905, 2023.

Skamarock, W. C., Klemp, J. B., Dudhia, J., Gill, D. O., Barker, D. M., Duda, M. G., Huang, X.-Y., Wang, W., and Powers, J. G.: A description of the advanced research WRF version 3, NCAR Technical Note, 475, 125, https://doi.org/10.5065/D68S4MVH, 2008.

Smagorinsky, J.: General circulation experiments with the primitive equations, Mon. Weather Rev., 91, 99–164, 1963.

Stanton, B. R.: Some oceanographic observations in the New Zealand fjords, Estuar. Coast. Shelf Sci., 19, 89–104, https://doi.org/10.1016/0272-7714(84)90054-4, 1984.

Stedmon, C. and Norman, N.: Chapter 10 – The Optical Properties of DOM in the Ocean, edited by: Hansell, D. A. and Carlson, C. A., Biogeochemistry of Marine Dissolved Organic Matter (Second Edition), Academic Press, 481–508, ISBN 9780124059405, https://doi.org/10.1016/B978-0-12-405940-5.00010-8, 2015.

Strickland, J. D. H.: Measuring the production of marine phytoplankton, published by the fisheries research board of canada under the control of the honourable the minister of fisheries, 122, 1960.

Strickland, J. D. H. and Parsons, T. E.: Determination of dissolved oxygen, A practical handbook of seawater analysis, 167, 71–75, 1968.

Takeoka, H.: Fundamental concepts of exchange and transport time scales in a coastal sea, Cont. Shelf Res., 3, 311–326, https://doi.org/10.1016/0278-4343(84)90014-1, 1984.

Taucher, J., Boxhammer, T., Bach, L. T., Paul, A. J., Schartau, M., Stange, P., and Riebesell, U.: Changing carbon-to-nitrogen ratios of organic-matter export under ocean acidification, Nat. Clim. Change, 11, 52–57, https://doi.org/10.1038/s41558-020-00915-5, 2020.

Tomas, C. R. (Ed.).: Identifying marine phytoplankton, Elsevier, ISBN 0080534422, 9780080534428, 1997.

Tomas, H., Ittekkot, V., Osterroht, C., and Schneider, B.: Preferential recycling of nutrients – the ocean's way to increase new production and to pass nutrient limitation?, Limnol. Oceanogr., 44, 1999–2004, 1999.

Thomson, R. E. and Emery, W. J.: Data Analysis Methods in Physical Oceanography, Elsevier, Waltham, Mass., ISBN 9780123877826, 2014.

Thomson, R. E., Spear, D. J., Krassovski, M. V., Hourston, R. A. S., Juhász, T. A., and Mihály, S. F.: Buoyancy-driven coastal current blocks ventilation of an anoxic fjord on the Pacific coast of Canada, J. Geophys. Res.-Oceans, 122, 2976–2998, https://doi.org/10.1002/2016JC012512, 2017.

Torres, R., Pantoja, S., Harada, N., González, H. E., Daneri, G., Frangopulos, M., and Fukasawa, M.: Air-sea $CO_2$ fluxes along the coast of Chile: From $CO_2$ outgassing in central northern upwelling waters to $CO_2$ uptake in southern Patagonian fjords, J. Geophys. Res.-Oceans, 116, C09006, https://doi.org/10.1029/2010JC006344, 2011.

Troupin, C., Machín F., Ouberdous M., Sirjacobs D., Barth A., and Becker J.-M.: High-resolution climatology of the northeast Atlantic using Data-Interpolating Variational Analysis (Diva), J. Geophys. Res., 115, C08005, https://doi.org/10.1029/2009JC005512, 2010.

Utermöhl, H.: Zur vervollkommnung der quantitativen phytoplankton-methodik: Mit 1 Tabelle und 15 abbildungen im Text und auf 1 Tafel, Internationale Vereinigung für theoretische und angewandte Limnologie: Mitteilungen, 9, 1–38, https://doi.org/10.1018/05384680.1958.11904091, 1958.

Vanhellemont, Q. and Ruddick, K.: Atmospheric correction of metre-scale optical satellite data for inland and coastal water applications, Remote Sens. Environ., 216, 586–597, https://doi.org/10.1016/j.rse.2018.07.015, 2018.

Vaquer-Sunyer, R., and Duarte, C. M.: Thresholds of hypoxia for marine biodiversity, P. Natl. Acad. Sci. USAs, 105, 15452–15457, https://doi.org/10.1073/pnas.0803833105, 2008.

Valdenegro, A., and Silva, N.: Caracterizacion oceanografica física y química de la zona de canales y fiordos australes de Chile entre el estrecho de Magallanes y cabo de Hornos (CIMAR 3 fiordo), Cienc. Tecnol. del Mar, 26, 19–60, 2003.

Verardo, D. J., Froelich, P. N., and McIntyre, A.: Determination of organic carbon and nitrogen in marine sediments using the Carlo Erba NA-1500 Analyzer, Deep Sea Res., 37, 157–165, https://doi.org/10.1016/0198-0149(90)90034-S, 1990.

Velinsky, D. J. and Fogel, M. L.: Cycling of dissolved and particulate nitrogen and carbon in the Framvaren Fjord, Norway: stable isotopic variations, Mar. Chem., 67, 161–180, https://doi.org/10.1016/s0304-4203(99)00057-2, 1999.

Wang, X., Olsen, L. M., Reitan, K. I., and Olsen, Y.: Discharge of nutrient wastes from salmon farms: environmental effects, and potential for integrated multi-trophic aquaculture, Aquacult. Env. Interac., 2, 267–283, https://doi.org/10.3354/aei00044, 2012.

Williams, P. I. and Robertson, J. E.: Overall planktonic oxygen and carbon dioxide metabolisms: the problem of reconciling observations and calculations of photosynthetic quotients, J. Plankton Res., 13, 153–169, https://doi.org/10.1093/oxfordjournals.plankt.a042366, 1991.

Yao, W. and Millero, F. J.: The chemistry of the anoxic waters in the Framvaren Fjord, Norway, Aquat. Geochem., 1, 53–88, 1995.

Zhang, J., Gilbert, D., Gooday, A. J., Levin, L., Naqvi, S. W. A., Middelburg, J. J., Scranton, M., Ekau, W., Peña, A., Dewitte, B., Oguz, T., Monteiro, P. M. S., Urban, E., Rabalais, N. N., Ittekkot, V., Kemp, W. M., Ulloa, O., Elmgren, R., Escobar-Briones, E., and Van der Plas, A. K.: Natural and human-induced hypoxia and consequences for coastal areas: synthesis and future development, Biogeosciences, 7, 1443–1467, https://doi.org/10.5194/bg-7-1443-2010, 2010.